Cerebral Cortex, June 2017;27: 3378–3396

doi: 10.1093/cercor/bhw270
Advance Access Publication Date: 6 September 2017
Original Article

ORIGINAL ARTICLE

The Tbr2 Molecular Network Controls Cortical Neuronal Differentiation Through Complementary Genetic and Epigenetic Pathways

Alessandro Sessa[1], Ernesto Ciabatti[1,†], Daniela Drechsel[2], Luca Massimino[1], Gaia Colasante[1], Serena Giannelli[1], Takashi Satoh[3], Shizuo Akira[3], Francois Guillemot[2], and Vania Broccoli[1,4]

[1]Stem Cell and Neurogenesis Unit, Division of Neuroscience, San Raffaele Scientific Institute, 20132 Milan, Italy, [2]The Francis Crick Institute, Mill Hill Laboratory, The Ridgeway, London NW7 1AA, UK, [3]Laboratory of Host Defense, Osaka University, Osaka 565-0871, Japan, and [4]CNR Institute of Neuroscience, 20129 Milan, Italy

Address correspondence to Vania Broccoli, Stem Cells and Neurogenesis Unit, Division of Neuroscience, San Raffaele Scientific Institute, Via Olgettina 58, 20132 Milan, Italy. E-mail: broccoli.vania@hsr.it. Website: www.vaniabroccolilab.com

[†]Present address: Medical Research Council Laboratory of Molecular Biology, Cambridge CB2 0QH, UK

Abstract

The T-box containing *Tbr2* gene encodes for a transcription factor essential for the specification of the intermediate neural progenitors (INPs) originating the excitatory neurons of the cerebral cortex. However, its overall mechanism of action, direct target genes and cofactors remain unknown. Herein, we carried out global gene expression profiling combined with genome-wide binding site identification to determine the molecular pathways regulated by TBR2 in INPs. This analysis led to the identification of novel protein–protein interactions that control multiple features of INPs including cell-type identity, morphology, proliferation and migration dynamics. In particular, NEUROG2 and JMJD3 were found to associate with TBR2 revealing unexplored TBR2-dependent mechanisms. These interactions can explain, at least in part, the role of this transcription factor in the implementation of the molecular program controlling developmental milestones during corticogenesis. These data identify TBR2 as a major determinant of the INP-specific traits by regulating both genetic and epigenetic pathways.

Key words: intermediate neural progenitors, neurogenesis, neurog2, Tbr2

Introduction

The mammalian cerebral cortex is a complex ensemble of several neuronal and glial subtypes that are radially arranged in six layers and tangentially organized in several operational domains. Excitatory principal neurons are the largest neuronal population in the cerebral cortex that arise during development in a stereotyped temporal order from a population of neuronal progenitors known as radial glial cells (RGCs). Neurogenesis has a bimodal behavior in the developing cortex, presenting a direct or indirect process, which depends by the presence or not of a second class of neural progenitors called intermediate (or basal) neural progenitors (INPs) (Noctor et al. 2004; Götz and Huttner 2005). During direct neurogenesis, one RGC divides asymmetrically to produce a daughter RGC and a neuron, while in the indirect process, the RGC generates one INP that moves into the subventricular zone (SVZ) where it

divides symmetrically one or few more times before differentiating into neurons.

Neural stem cells (NSCs) maintain features of RGCs when cultured in vitro and have enabled the dissection of the molecular events that regulate RGC identity, self-renewal and proliferation dynamics (Muzio et al. 2002; Konno et al. 2008; Asami et al. 2011; Postiglione et al. 2011). In contrast, little is known on the genetic components regulating the INPs that lack a corresponding in vitro cell counterpart (Conti and Cattaneo 2010).

The transcription factor *Tbr2* (NCBI: *Eomes*) is one of the major intrinsic determinants of the INPs (Noctor et al. 2004; Hevner et al. 2006). In fact, others and we have described its essential role in INP identity during cortical and hippocampal development using loss- and gain-of-function approaches (Arnold et al. 2008; Sessa et al. 2008, 2010; Hodge et al. 2012; Kahoud et al. 2014). Importantly, *Tbr2* inactivation leads to an important decrease in the INP number and, in turn, in the final number of excitatory neurons in the cerebral cortex. These findings are consistent with the microcephalic manifestations occurring in patients with a *TBR2* gene deletion (Baala et al. 2007). Recently, in vivo tracing of the Tbr2+ NPC lineage revealed that virtually all cortical glutammatergic neurons transit through a Tbr2+ intermediate state during their development (Vasistha et al. 2015), confirming previous observations in Tbr2 mutant mice (Pontious et al. 2008; Sessa et al. 2008; Kowalczyk et al. 2009). Together with the RGCs located far from the ventricle (outer or basal RGCs), TBR2+ INPs are the major cellular component of the recently characterized outer subventricular zone (OSVZ), a morphological hallmark of girencephalic cortices as those of primates and humans (Fietz et al. 2010; Hansen et al. 2010; Reillo et al. 2011; Reillo and Borrell 2012; Florio et al. 2015). Beyond the leading role of the outer RGCs in promoting cortical foldings, the concomitant increase in TBR2+ INPs and their heightened proliferation potential might indicate a significant contribution of these cells in the evolutive cortical expansion (Martínez-Cerdeño et al. 2016). Accordingly, increasing number of TBR2+ INPs leads in mice to a significant enlarged cortical surface area, while in ferrets in the formation of additional folds and fissures (Nonaka-Kinoshita et al. 2013). In addition, a large scale transcripto mic study in gyrencephalic species highlighted the relevance for *Tbr2* in the OSVZ for promoting and sustaining cerebral cortical expansion and folding (de Juan Romero et al. 2015).

Despite the increasing role of INPs in cortical development and evolution, the understanding of the Tbr2 molecular network has remained limited (Elsen et al. 2013). Herein, we sought to undertake a genomic approach to decipher the TBR2 dependent molecular mechanisms controlling both morphological and functional features of INPs. To this end, we generated and cross-referenced datasets of the Tbr2-dependent expression profiling and its genomic binding profile. Through this systematic survey, we identified numerous Tbr2 target genes, which have a role in shaping the morphology and behavior of INPs from their genesis to long-term maintenance. Importantly, we revealed that TBR2 exerts its functions in either controlling the expression of target genes directly or modulating the action of other regulatory proteins. In fact, we identified its cooperation with the proneural transcription factor NEUROG2 and the histone demethylase JMJD3 (NCBI: KDM6B). In particular, TBR2 directs JMJD3-dependent chromatin remodeling to specific genomic targets to enable the removal of H3K27me3 chromatin mark. Altogether, this genomic analysis reveals the complex molecular program regulated by TBR2 for the correct establishment of the cortical neuronal differentiation process through both genetic and epigenetic mechanisms.

Materials and Methods

Animals

Tbr2 conditional mutant mice (Tbr2flox/flox, Tbr2 cKO) (Mao et al. 2008) were maintained by backcrossing with C57Bl/6 animals. To inactivate Tbr2 in the developing forebrain, Tbr2flox/flox mice were crossed with Tbr2flox/+; Foxg1-Cre animals (Hébert and McConnell 2000). Genotyping was performed as described previously to distinguish wild-type, floxed, and deleted Tbr2 alleles (Mao et al. 2008). Mice were maintained at the San Raffaele Scientific Institute Institutional mouse facility, and experiments were performed in accordance with experimental protocols approved by local Institutional Animal Care and Use Committees (IACUC).

RNA Isolation, Processing and Microarray Analysis

E14.5 embryos from Tbr2flox/flox × Tbr2flox/+; Foxg1-Cre were harvested and placed into cold PBS. After brain isolation, meninges and olfactory bulbs were removed, and the cerebral cortex separated from the ventral telencephalon. The same procedure was repeated for 3 control (Tbr2flox/+; Foxg1-Cre) and 3 Tbr2 mutant (Tbr2flox/flox; Foxg1-Cre) embryos. Total RNA was extracted from the tissues by using the Qiagen RNA micro kit (Qiagen, Valencia, CA) and cRNAs generated and hybridized on a total of six different MOE430v2 Affymetrix DNA chips according to the Affymetrix protocol. The chips were scanned (Affymetrix) to generate digitized image data files. The data were deposited in the NCBI Gene Expression Omnibus (Edgar et al. 2002) and are accessible through GSE63621.

Microarray Data Analysis

Microarray quality control and statistical validation were performed using Bioconductor (Gentleman et al. 2004; Sanges et al. 2007). Background correction, normalization, and probe set intensities were obtained by means of GCRMA (Wu and Irizarry 2004). To assess differential expression we performed two-sample *t*-test to rank differentially expressed genes between Tbr2 mutants and controls. We compensate multiple testing and compute false discovery rate (FDR) using beta-uniform mixture model (BUM) (Pounds and Morris 2003). Gene Ontology (GO) analysis was performed using DAVID (http://david.abcc.ncifcrf.gov) (Huang et al. 2009).

Quantitative Real-Time PCR and Quantification

About 2 μg of the total RNA extracted from Ctrl and Tbr2 mutant dorsal telencephali were reverse transcribed with random hexamers as primers using a Thermoscript RetroTranscriptase (Invitrogen). Oligonucleotide primers for the amplification of the selected genes are reported in Table S3. qPCRs were carried out in a final volume of 25 μl, containing a concentration of 100 nM of each primer, 1× Syber Green supermix (Biorad) and 2 μl of the RT products. Thermal cycling was performed using a Mx3005 P QPCR system (Stratagene). Melting curve analysis was performed for each reaction to ensure a single peak and amplicons were visualized after electrophoresis on a 2% agarose gel to ensure the presence of a single PCR product.

The Livak method was applied for quantification (Schmittgen and Livak 2008). Briefly, the expression of each gene either in wild-type or in mutant samples was normalized to that of the housekeeping gene β-actin: to this purpose a ΔCT, WT = (CT, gene – CT, act)WT and a ΔCT, MUT = (CT, gene – CT, act)MUT were calculated for each amplified gene and results reported as fold change (2-ΔΔCT) in gene expression of Tbr2 mutant samples relative to the wild-type, where – ΔΔCT = – (ΔCT, MUT – ΔCT,WT). The data were plotted as means of at least three animals per genotype (biological replicates) and three independent amplifications (technical replicates). Error bars represent standard error of the mean.

In Situ RNA Hybridization

ISHs on frozen sections were performed as previously described by Schaeren-Wiemers and Gerfin-Moser (1993) with the following modifications. Sections were fixed for 30 min at room temperature in 4% paraformaldeyde in PBS and treated for 5 min with 1 μg/ml proteinase K in 1 mM EDTA, 20 mM Tris-Hcl (pH7.0). Prior to hybridization, they were washed twice in 2× SSC for 15 min, and incubated in 0.1 M Tris/0.1 M of glycine for at least 30 min. The hybridization solution (60 μl/slide) contained 50% formamide, 5× SSC (pH adjusted with citric acid to pH6.0), 5% dextran sulfate, 2 mg/ml heparin, 100 μg/ml tRNA and from 1:100 to 1:50 dilution of the riboprobes, and was performed overnight at 65 °C using coverslips. Next, the sections were washed for 1–2 h in 0.5× SSC, 20% formamide at 65 °C. Subsequently, they were treated with 10 μg/ml RNaseA for 30 min at 37 °C in NTE, then washed for 4 h in 0.5× SSC, 20% formamide a 65 °C and for 30 min in 2× SSC, and blocked for 1 h at room temperature in 1% blocking reagent (Roche, Switzerland) in MABT. A 1:5000 dilution of anti-digoxigenin-AP conjugated antibody (Roche) was preincubated for at least 1 h in 1% blocking reagent in MABT at 4 °C. Slices were incubated with the antibody overnight at 4 °C, washed for 6 h in TBST, for 30 min in NTMT, and stained using centrifuged BM purple AP substrate (Roche) in 0.3% Tween-20 for 12–36 h at 4 °C or room temperature. Slices were washed in NTMT, then in distilled water, and mounted in Aquamount (Polysciences). The following probes were used: *Ebf1, Ebf2, Ebf3* (kindly provided by Dr Giacomo Consalez), *Gbx2, Rnd2, Jmjd3, Sox5, Tle4, Math2*.

Chromatin Immunoprecipitation

E14.5 cortices (dissected in cold HBSS) or NSCs were fixed 45' in PBS containing 2 mM di-succinimidyl-glutarate (DSG). After washing with PBS, protein–DNA interactions were fixed by 10 min incubation in 1% formaldehyde at room temperature. Crosslinking was then quenched by addition of glycine to a final concentration of 125 mM Glycin. Subsequently, cells were washed in PBS, harvested by scraping, and resuspended in SDS lysis buffer (1% SDS, 10 mM EDTA, 50 mM Tris), containing protease inhibitors (Roche). The chromatin was sheared by sonication using a Bioruptor (Diagenode) sonicator for 25–30 min in 30 s ON/OFF cycles. Samples were centrifuged at 1600× *g* to remove debris and the DNA-concentration was determined using a Nanodrop Spectrophotometer. Immunoprecipitations with mouse anti-Tbr2 (AbCam #ab23345), anti-Neurog2 (generous gift of Yong Chao Ma and Mike Greenberg) or control GFP antibodies (Molecular Probes #6455) were done as described (Castro et al. 2011) using 80 μg of chromatin and 2 μg of antibody per assay. DNA sequences were quantified by real-time PCR (primers are listed in Table S3). Quantities of immunoprecipitated DNA were calculated by comparison with a standard curve generated by serial dilutions of input DNA. The data were plotted as means of at least two independent ChIP assays (biological replicates) and three independent amplifications (technical replicates). Error bars represent standard error of the mean.

ChIP-sequencing

Tbr2 and Neurog2 ChIP samples were sequenced with Illumina Genome Analyzer IIx. ChIP-seq data analysis was performed with the GeneProf web-based software (Halbritter et al. 2012, 2014). Sequences with a Mean Quality Score > 10 were aligned to the mm9 reference genome with Bowtie v0.12.3. ChIP peaks were called with MACS v1.4 (Bandwidth = 200; FDR < 0.1) and adjusted with the dynamic λ calculation to account for the potential local bias imposed by chromatin structure. Tracks were displayed on the reference genome with the IGV software (Thorvaldsdóttir et al. 2013). Statistical enrichments for associations between genomic regions and functional annotations were performed with GREAT (McLean et al. 2010). The GEO accession number for the ChIP-seq data reported in this paper is GSE63621.

In Utero Electroporation

Electroporation in utero was employed to deliver expression vectors to the ventricular RGCs of mouse embryos as previously described (Gal et al. 2006; Saito 2006). Briefly, uterine horns of E12.5 or E13.5 pregnant dams were exposed by midline laparotomy after anesthetization with Avertin (312 mg/kg). One microliter of DNA plasmid corresponding to 3 μg mixed with 0.03% fast-green dye in PBS was injected in the telencephalic vesicle using a pulled micropipette through the uterine wall and amniotic sac. Platinum tweezer-style electrodes of 7mm were placed outside the uterus over the telencephalon and 5 pulses of 40 V, 50 ms in length, were applied at 950 ms intervals by using a BTX square wave electroporator. The uterus was then replaced in the abdomen, the cavity was filled with warm sterile PBS and the abdominal muscle and skin incisions were closed with silk sutures.

Organotypic Culture and Focal Electroporation

E14.5 embryonic mouse midbrain were isolated, embedded in 4% low-melting agarose (Sigma) and 250 μm thick coronal sections were cut using a vibratome (VT1100, Leica). The sections were then transferred to polycarbonate culture membranes (diameter, 13 mm; pore size 8 μm; Costar) in organ tissue dishes containing 1.5 ml of serum-containing medium (Gibco a-MEM with 10% fetal calf serum, glutamine, penicillin and streptomycin). Slices were maintained for 1 h at 37 °C in 5% CO_2 in a standard sterile incubator. Before changing to the Neurobasal/B27 (Gibco) medium, 1 μl of DNA plasmid corresponding to 5 μg mixed with 0.03% fast-green dye in PBS was mouth-injected in the area of interest and the same area was electoporated with a square-electroporator (ECM830, BTX, Holliston, MA) using planar electoctodes (BTX) and applying 2 electric pulses of 100 V for 5ms as described by Stühmer et al. (2002). Organotypic slices were maintained for 2 days in vitro and then fixed in 4% PFA in PBS, cryoprotected in 30% sucrose, embedded in OCT coumpond, and resectioned on a cryostat (10 μm) for immunohistochemistry.

Immunohistochemistry

Immunohistochemical analyses were performed as described previously (Colombo et al. 2004). Briefly, frozen or paraffin sections were boiled in 10 mM sodium citrate, pH 6.0 and blocked in 10% normal goat serum (NGS) and 0.2% Triton-X-100 for 1 h at room temperature. Incubation with primary antibodies was performed at 4 °C overnight. Secondary antibodies were applied to sections for 2 h at room temperature. The primary antibodies utilized were as follows: rabbit anti-Tbr2 (1:200, Chemicon), chicken anti-GFP (1:500, Invitrogen), rat anti-BrdU (1:200, Biorad), anti-KI67 (1:100, Immunological Science), anti-Satb2 (1:200, AbCam), anti-Tle4 (1:100, Santa Cruz), Tbr1 (1:100, Abcam). Secondary antibodies were conjugates of Alexa Fluor 488, Alexa Fluor 594, and Alexa Fluor 647 (1:500) or biotin (1:200). DAPI (4',6'-diamidino-2-phenylindole) was used as nuclear counterstaining. Finally, slices were washed and mounted in Fluorescent Mounting Medium (Dako Cytomation).

Quantification and Statistical Analysis

Data collection and analysis were performed blind to genotype and the experimental conditions, data were collected and processed randomly. No statistical methods were used to predetermine sample sizes which were comparable to those reported in previous publications (Sessa et al. 2008, 2010) and based on previous knowledge of the variability associated with the different experiments. At least three serial sections from three different animals for each genotype (biological replicats) were photographed using a Nikon Eclipse 600 fluorescent microscope. Each single experiment were repeted three times (technical replicats). Images were imported into Photoshop CS6. EGFP-only, marker-only, and/or double-positive cells were overlaid manually by color-coded dots in new layers. The number of labeled cells (dots) was calculated using the record measurements of Photoshop CS3 and imported into Excel 2008. The total number of labeled cells per field per section was calculated across all brains. Results were expressed as the mean value of marker+ cells per field ± SEM and were tested for statistical significance by the one-tailed Student's t-test for paired differences with GraphPad Prism software. For the distribution of the marker+ cells in the cortical wall: the entire coronal section of the cortex was divided arbitrarily in four, six or eight bins (according to the developmental stage) and positive cells were counted per bin. Results were expressed as the percentage of the marker+ cells per bin on total marker+ cells per section and were tested for statistical significance by the one-tailed Student's t-test for paired differences with GraphPad Prism software.

Luciferase Reporter Assay

P19 cells (ATCC) were seeded in Minimum Essential Medium Eagle Alpha (Sigma-Aldrich) with 7.5% bovine calf serum and 2.5% fetal bovine serum. They were transfected 24 h after plating with 400 ng of each of the following constructs in different combinations: pT81 luciferase reporter plasmids, control plasmid pCAGiresGFP, pCAGArx-iresGFP, pCDNA3-Tle1, and 80 ng of pRL-TK-Renilla luciferase plasmid DNA (Promega) using Lipofectamine LTX with Plus Reagent (Life Technologies). Forty-eight hours post-transfection, cells were lysed and measurement of firefly and Renilla luciferase activity was performed using the Dual-Glo Luciferase Assay System (Promega) in a GloMax 20/20 Luminometer (Promega) according to the manufacturer's instructions. The firefly luciferase activity was normalized according to the corresponding Renilla luciferase activity, and the final LUC activity was reported as mean relative to pCAG-iresGFP/luciferase transfection. Each condition was repeated three times and each lysate was read three times independently. Primers used to clone the regions used as driver are reported in Table S3.

NSC Cultures

Embryonic cortices were dissociated, fragmented in Hank's Balanced Salt Solution (HBSS, Life Technologies) with 1% Penicillin/Streptomycin (Sigma-Aldrich) and digested with papain (10 U/ml, Worthington Biochemical) and cysteine (1 mM, Sigma-Aldrich) in HBSS with 0.5 mM EDTA at 37 °C. The obtained NSCs were routinely cultured in suspension as neurospheres.

Hippocampal Cultures

Primary neuronal cultures were prepared from the hippocampi of E17.5 mouse embryos. Briefly, hippocampi were dissected from mouse brains under a dissection microscope and treated with trypsin (Invitrogen) for 15 min at 37 °C before triturating mechanically with fire-polished glass pipette to obtain a single-cell suspension. Approximately 7×10^4 cells were plated on coverslips coated with poly-L-lysine in 12-well plates and cultured in Neurobasal medium (Invitrogen) supplemented with B27 (Invitrogen) and glutamine (Sigma-Aldrich). Neurons were transfected 2 days after plating with $CaCl_2$ method and fixed for immunostaining 3 days after.

Results

Loss of *Tbr2* Causes a Significant Alteration of Gene Expression in the Developing Cerebral Cortex

To investigate the impact of *Tbr2* inactivation on the cortical neuronal gene expression program, we initially determined the differentially expressed genes between Tbr2 mutant and control cortices (Sessa et al. 2008). Microarray-based transcriptome analysis was performed at E14.5 in order to detect early differences in expression profiling before the appearance of evident morphological changes in Tbr2 mutant brains (Sessa et al. 2008). By this approach, we identified about 2200 differentially expressed genes which cluster in two groups of equally represented up and down-regulated genes in Tbr2 mutant compared with control cortices (Fig. 1A–C). Interestingly, functional enrichment analysis revealed that the majority of them belong to GO categories mostly relevant for the nervous system development (Figure S1A and Table S2A). In particular, *Tbr2* gene loss caused a reduced expression of critical molecular determinants in corticogenesis like *Tbr1*, *Mef2*, *Bcl11b*, *Satb2* and *Zfp238* (Fig. 1D). Conversely, most upregulated genes showed that TBR2 is necessary to suppress genes that are not physiologically expressed in the cerebral cortex, but are present either in neighbor areas, such as the ventral telencephalon (i.e., *Ebf1,2,3*, *Otx2* and *Gbx2*), or even in more distal regions as Tyrosine Hydroxylase (*Th*) (Fig. 1E). Interestingly, all these genes presented a similar pattern of ectopic expression coinciding exactly with the SVZ region, the area where the INPs reside throughout the different stages of development (from E12.5 to E18.5) (Fig. 1F, Figure S1B and data not shown). Thus, these results suggest that upon Tbr2 loss, INPs undergo a process of molecular miss-specification rather than disappearance as they acquire the expression of genes encoding for transcription

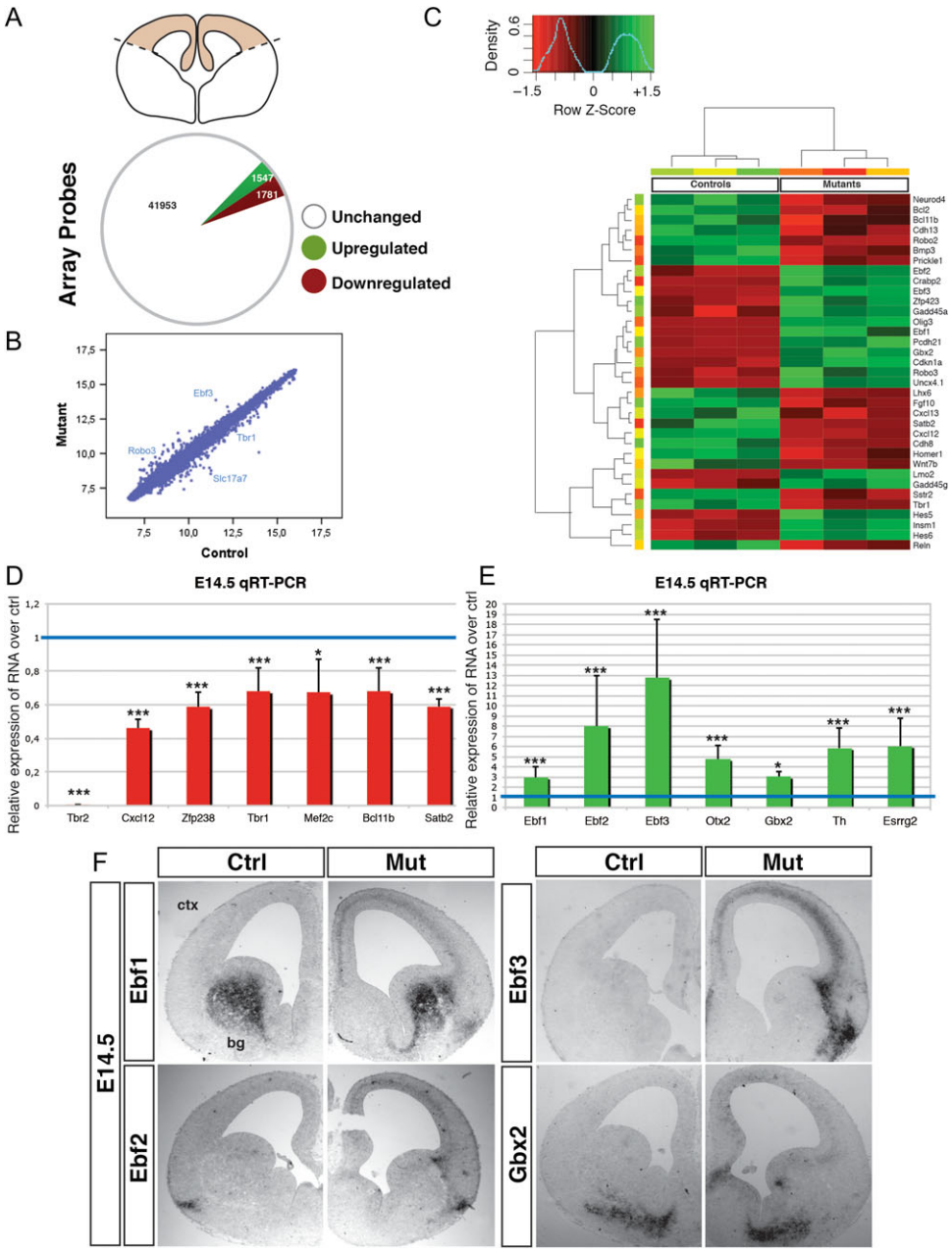

Figure 1. Tbr2 gene loss leads to massive transcriptional alterations in the developing cortex. (*A*) Upper part: schematic view showing the dorsal telencephalon isolated for transcriptome analysis. Bottom part: graph with the 1547 microarray probes upregulated and 1781 down-regulated in Tbr2 mutants compared with controls. (*B*) Scatter plot of array probe mean values in mutants and controls. (*C*) Heat-map of gene expression changes for selected genes with pure green, black and red indicating high, medium and low levels of gene expression, respectively. (*D*, *E*) qPCR analysis on independent control and mutant cortical samples for genes either down-regulated (*D*) or upregulated (*E*) in Tbr2 cKO. Bars indicate SD. (*F*) In situ hybridization experiments on coronal section of E14.5 control and Tbr2 mutant forebrains revealing the ectopic expression of the genes Ebf1, Ebf2, Ebf3 and Gbx2 in the Tbr2 mutant cortical SVZ domain. * = t-test, $P < 0.05$; *** = t-test, $P < 0.001$. ctx = cerebral cortex, bg = basal ganglia.

factors involved in the specification of alternative neuronal subtypes (Fig. 1*E*) (Kovach et al. 2013). To confirm the ability of Tbr2 to suppress alternative cell fates, we electroporated E13.5 organotypic slices to force its expression in the ventral mesencephalon. Two days later, *Tbr2* ectopic expression was found to strongly reduce TH protein that, conversely, was detectable in control (GFP electroporated) slices (Figure S1C). Altogether, these results confirmed the critical action of TBR2 in preventing the activation of spurious genes in INPs, including those coding for relevant developmental factors of different neuronal cell types, thus contributing to the correct specification of cortical INP cells.

TBR2 Binds and Regulates Different Classes of Developmental Related Genes

To determine the genome-wide TBR2 binding occupancy, we combined chromatin immunoprecipitation with massive deep sequencing (ChIP-seq). To preserve at best its biological significance, ChIP was performed on chromatin directly isolated from

E14.5 dorsal telencephali using a validated TBR2 antibody. The subsequent sequence analysis uncovered >14.000 distinct DNA regions (false discovery rate, FDR, <5%) that were categorized in accordance with their position in the genome (Fig. 2A). The vast majority were mapped in distal intergenic regions (50%) or in known introns (31%) while less peaks were identified in regions considered to be gene promoters (<2 kb and 2–20 kb upstream of transcription start site TSS, 5% and 11% respectively) suggesting a regulation of gene expression mainly independent from proximal promoters. Remarkably, these

Figure 2. Characterization of the transcriptional program regulated by Tbr2 in the dorsal telencephalon. (*A*) Pie chart illustrates genomic location of the ChIP-Seq peaks: promoters (<2000 bp from TSS) 5%, 20 kb upstream regions (>2000 bp and <20 kb from TSS) 11%, exons 3%, introns 31%, intergenic regions (>20 kb from TSS) 50%. 14 539 unique regions (FDR < 0.1) are sorted according to TBR2 occupancy (vs. GFP antibody as control). (*B*) Motif search using MEME software identified the T-box consensus binding site on the selected sequences. The table indicates the occurrence of the T-box motif in the dataset. Bottom: The graph indicates the distributions of either the total number of TBR2 peaks (blue bars) or only the peaks containing T-box motif (red bars) respect to the distance from the TSS. (*C*) GO biological process terms in genes associated (the nearest TSS) with Tbr2 bound genomic regions for all peaks (left), or those within 0–2 kb from the TSSs (right, up), within 2–20 kb from the TSSs (right, middle) and >20 kb from the TSSs (right, bottom). (*D*) qPCR analysis on independent ChIP samples (using anti GFP or anti-Tbr2 antibodies) of Tbr2 bound regions associated with genes normally expressed in ventricular zone (VZ), SVZ, CP or marginal zone (MZ) or in a complex manner in the developing cortex (Complex) or elsewhere (Alter). ORF1 is a negative control genomic region. Quantification in triplicate from at least two immunoprecipitation samples, mean ± SEM. (*E*) Venn diagram showing the overlap between the TBR2 bound genes (blue) and the genes up- (green) and down-regulated (red) in Tbr2 mutant cortex. (*F–H*) Luciferase assays showing that TBR2 directly represses (*F*), activates (*H*) or has no effect (*H*) on regulatory regions identified by ChIP-Seq and associated with genes relevant for cortex development. * = t-test, $P < 0.05$; *** = *t*-test, $P < 0.001$; N.S. = *t*-test, $P > 0.05$.

sequences shared a putative DNA-binding site for T-box proteins, confirming the accuracy of the identified binding events (MEME web-tool dataset, Fig. 2B) (Sinha et al. 2000; Naiche et al. 2005). A large fraction of peaks (36%) contains the T-box motifs whose distribution with respect of the closest TSS matches that of the whole peak profile (Fig. 2B). To validate these results, independent ChIP-qPCR experiments were performed on candidate target regions confirming their robust enrichment in Tbr2- versus GFP-immunoprecipitated chromatin (Figures S2A and D). Antibody specificity was confirmed by the lack of qPCR amplification in TBR2 ChIP-qPCR experiments in Tbr2 KO tissues (Figure S2A). Tbr2 bound genomic regions were assigned to their nearest genes and interrogated by GO for their biological functions. Significantly, the most enriched biological processes included regulation of cell proliferation, cell migration and differentiation, all correlated with events occurring during cortical development (Fig. 2C and Tables S2B–E). We, then, stratified these genes for their expression pattern in E14.5 telencephalon according to available databases (www.genepaint.org; www.brain-map.org.). In this analysis, we identified putative Tbr2 target genes expressed exclusively in proliferative (VZ + SVZ) or differentiated (Cortical Plate, CP) regions or in both as well as genes with a more complex expression pattern (Figure S2B), suggesting a broad impact of TBR2 during corticogenesis.

To evaluate the impact of TBR2 in controlling the expression of its putative target genes, we crossed the ChIP-seq dataset (gene was called if the peak is <30 kb upstream or <1 kb downstream from the TSS) with the genes exhibiting a deregulated expression in *Tbr2* mutants (Fig. 2E). From this analysis, we obtained a list of 175 putative direct targets that were upregulated in *Tbr2* deficient cortex and thus possibly repressed by TBR2, and 267 that could be directly activated (Fig. 2E, Table S1B). Notably, the ChIP peaks related to these genes presented a consistent shift towards intronic regions in their distribution compared with the total peak distribution (Figure S2E). To experimentally test whether these genes were directly regulated by TBR2, we cloned different regulatory sequences of the selected misregulated genes previously validated by ChIP-qPCR and then assessed the direct transcriptional ability of TBR2 using promoter luciferase report assays (Fig. 2F–H and Figure S2C). Interestingly, TBR2 was able to activate *Reelin, Fezf2* and *Satb2* regulatory regions while repressing those associated with the *Gadd45g* and *Hes5* genes (Fig. 2F, G, Figure S2C). However, regulatory regions of other candidate genes were found to be insensitive to TBR2 (Fig. 2H, Figure S2C). These negative findings might implicate the lack of the necessary cofactors or the appropriate chromatin architecture to enable the TBR2 function in P19 cells, or alternatively, the ancillary role of TBR2 in regulating the expression of some of its target genes. Certainly, these results might provide an explanation for the seemingly low grade of intersection between the ChIP-Seq and expression profile datasets (Fig. 2E).

NEUROG2 Shares with TBR2 a Large Fraction of Binding Sites Along the Genome

We then explored the possibility that TBR2 can act synergistically with other transcription factors on some of its target genes. On this view, *Neurogenin-2* (*Neurog2*) is a plausible candidate since it is a key determinant of the cortical excitatory neuronal lineage, promotes INP differentiation and exhibits a highly overlapping expression pattern with *Tbr2* in the developing cortex (Fode et al. 2000; Noctor et al. 2004; Sessa et al. 2008; Kovach et al. 2013). Thus, we performed ChIP-Seq for NEUROG2 on E14.5 dorsal telencephali using an anti-NEUROG2 specific antibody identifying 2640 distinct genomic peaks located mainly in intergenic (48%) and intronic (30%) regions (Fig. 3A). We were able to identify from this dataset a consensus for the E-box, the DNA sequence recognized by bHLH factors including Neurogenins (Bertrand et al. 2002) present in the 36% of the peaks which showed the same distribution with respect to TSS of the total set (Fig. 3B). Intriguingly, a T-box consensus domain was identified in the same sequences suggesting the possibility that these regions could be bound by both factors together (Fig. 3B). The results were verified by independent ChIP experiments confirming the enrichment in NEUROG2 compared with GFP (control) immunoprecipitated chromatin (Figure S3A). The 1534 genes identified as NEUROG2 targets included genes previously showed to be authentic NEUROG2 downstream effectors (e.g. *Neurod1* and *Rnd2*) (Huang et al. 2000; Heng et al. 2008) (Figure S3A) and classified in GO categories closely related with neurogenesis (Fig. 3C and Tables S2F–I).

The comparison between the genomic regions identified in Tbr2 and Neurog2 ChIP-Seq analyses revealed that the vast majority of the Neurog2 associated sequences overlaps with TBR2 bound regions (Fig. 3D and Table S1C). This finding was confirmed by independent ChIP assays performed on shared regions randomly chosen from the overlay of the datasets (Fig. 3E). In TBR2/NEUROG2 common peaks we found high occurrence of both E- and T-box motifs (Figure S3B). Of note, the peaks containing both E- and T-boxes have a tendency to localize closer to the TSS respect to the total common regions (Figure S3B). These results prompted us to test for a possible interaction between NEUROG2 and TBR2 at protein level. Interestingly, NEUROG2 was detected in the TBR2 immunoprecipitated fraction of E14.5 cortical extracts (Fig. 3F). These data suggest that the two proteins can assemble in the same complex, although do not necessary indicate their functional cooperation on gene regulation. To answer to this last issue, we selected regions upstream to *Sox11* and *Neurod4* (Fig. 3G and Figure S3B, respectively) where common peaks in Tbr2 and Neurog2 datasets were identified, and verified the individual binding of each of the two TFs by independent ChIP experiments (Fig. 3H and Figure S3C). Subsequently, the two regions were cloned upstream to a minimal promoter for luciferase transcriptional assays (Fig. 3I and Figure S3D). For the Sox11 enhancer, the action of either *Tbr2* or *Neurog2* alone triggered a 4–5 fold activation, while the two TFs together burst the expression to 14-fold over the basal level, thus demonstrating a strong positive synergic activity (Fig. 3I). However, the effect of cooperation between the two TFs was different for the *Neurod4* enhancer (Figure S3D). In this case, *Tbr2* did not elicit any effect alone, but was sufficient to counteract the strong activation mediated by *Neurog2* (Figure S3E). Interestingly, both targets are negatively regulated in Tbr2 mutant cortices (Fig. 3J and Figure S3G). A similar finding was obtained when the *Neurod1* promoter, containing both TBR2 and NEUROG2 bound regions, was tested (Figure S3H–K). In fact, the significant activation of the reporter gene by NEUROG2 resulted almost completely abolished by TBR2 coexpression (Figure S3I). This result is consistent with the increase expression level of *NeuroD1* in *Tbr2* mutant cortices (Figure S3L). Taken together, these data revealed a conserved functional cooperation of TBR2 and NEUROG2 on multiple target genes where their specific role might be synergic or opposite depending by the gene locus.

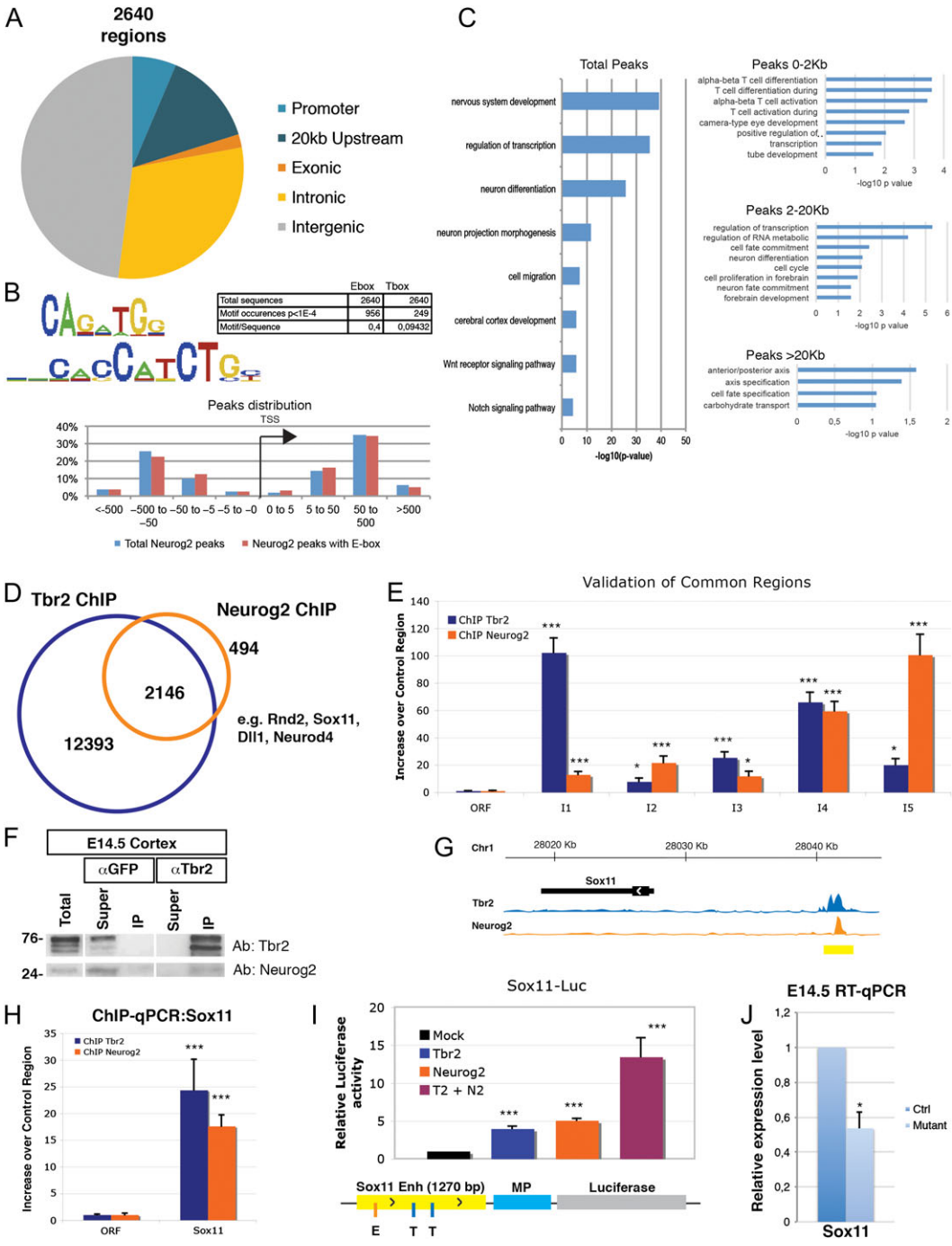

Figure 3. TBR2 and NEUROG2 interact to control neurodevelopmental gene programs. (*A*) Pie chart illustrates genomic location of ChIP-Seq peaks: promoters (<2000 bp from TSS) 6%, 20 kb upstream regions (>2000 bp and <20 kb from TSS) 14%, exons 2%, introns 30%, intergenic regions (>20 kb from TSS) 48%. 2643 unique regions (FDR < 0.1) are sorted according to NEUROG2 occupancy (vs. GFP antibody as control). (*B*) Motif enriched in NEUROG2-bound segments predicted by MEME software identified E-box and T-box consensus binding sites. Table represents the occurrence of E-box or T-box motif in the dataset. Bottom: Graph indicating either the distributions of the total number of TBR2 peaks (blue bars) or the peaks containing the E-box motif (red bars) respect to the distance from the TSS. (*C*) Enrichment of GO biological process terms in genes associated (the nearest TSS) with NEUROG2 bound regions for all peaks (left), or those within 0–2 kb from the TSSs (right, up), within 2–20 kb from the TSSs (right, middle) and >20 kb from the TSSs (right, bottom). (*D*) Venn diagram showing the overlap between genes associated with NEUROG2- (orange) or TBR2 bound regions (blue). (*E*) qPCR analysis on independent Tbr2 or Neurog2 ChIP samples for DNA regions randomly chosen from peaks shared between ChIP-seq datasets. ORF is negative control region. Quantification in triplicate from at least two immunoprecipitation experiments. Mean ± SEM. (*F*) Endogenous immunoprecipitation using anti-Tbr2 antibody (or anti-GFP as control) performed on E14.5 dorsal forebrain protein extracts reveals that TBR2 and NEUROG2 are in the same physical complex. (*G*) Visualization of Tbr2 (blue track) and Neurog2 (orange track) ChIP-seq peaks in Sox11 genomic locus. (*H*) qPCR analysis on independent Tbr2 and Neurog2 ChIP experiments for the region containing Tbr2 and Neurog2 overlapping peaks near to Sox11 gene. ORF is negative control region. Quantification in triplicate from at least two immunoprecipitation experiments. Mean ± SEM (*I*) Luciferase assay using the same region (Sox11 Enh, 1270 bp) tested in H using Tbr2, Neurog2 and the two TFs together. E-box (as E) and T-boxes (as T) sequences are indicated in the luciferase expressing vector. (*J*) Expression data obtained by RT-qPCR assays of Sox11 in control and Tbr2 mutant cortices. MP = minimal promoter. * = t-test, $P < 0.05$; *** = t-test, $P < 0.001$.

TBR2 Synergizes with NEUROG2 to Control Radial Migration by Modulating *Rnd2* Expression

One crucial process during cerebral cortex formation is the timely radial migration of newly generated postmitotic neurons in the outward direction towards their final location (Ayala et al. 2007). Considering that a number of genes with a role in cell motility are apparently regulated by TBR2 (Fig. 2C and Table S2C), we asked whether TBR2 has a function in modulating radial migration. In line with this possibility, *Tbr2* gene expression is found higher in neural progenitors settled in the SVZ while rapidly decreases once they initiate radial migration (Noctor et al. 2004). To investigate this issue, we developed two different approaches to ectopically express *Tbr2* exclusively in migrating neuron precursors, while leaving unperturbed the RGCs (Sessa et al. 2008). First, in utero electroporations were conducted (Saito 2006) with a construct in which *Tbr2* and/or GFP expression was driven by the *Neurod1* promoter specifically in postmitotic neurons (Miyoshi and Fishell 2012) (Fig. 4A). Two days after surgery, GFP^+ electroporated (control) cells were found scattered between the IZ (reflecting the endogenous *Neurod1* expression) (Hevner et al. 2006) and the cortical plate, while *Tbr2* overexpressing cells remained abnormally stacked within the IZ (Fig. 4A). Notably, 5 days after electroporation control cells were correctly located in the most superficial layers of the cortical plate, while the *Tbr2* overexpressing cells were spread throughout the cortical wall, thus indicating a delayed and defective radial migration pattern (Fig. 4A). In the second approach, we employed a tamoxifen inducible construct for the timely activation of *Tbr2* expression after in utero electroporation (Figure S4A). We found that the administration of 4-OHT at E14.5, 24 h after plasmid in vivo delivery, enabled to evaluate the *Tbr2* overexpression in different subsets of cells according to their position at the time of the electroporation (e.g. apical region vs. basal) (Figure S4A). Notably, the block of migration resulting from *Tbr2* overexpression was also evident in this experimental system, with ectopic masses of cells stacked in SVZ-IZ compared with the control (Figure S4A). In search for a molecular mechanism regulating this effect, we identified in the ChIP-Seq datasets candidate binding sites for TBR2 and NEUROG2 in the enhancer region of the *Rnd2* gene coding for a small GTP-binding protein with a key role in radial migration (Fig. 4B, C) (Heng et al. 2008). To explore whether and to what extent TBR2 and NEUROG2 control *Rnd2* expression, we employed a luciferase reporter plasmid containing the *Rnd2* enhancer/promoter element and verified its dependence by the two factors (Fig. 4D). As already reported, NEUROG2 was more efficient than TBR2 to induce transcriptional activity (16-fold vs. 5-fold over basal level, Fig. 4D) (Heng et al. 2008). However, equal coexpression of *Neurog2* and *Tbr2* led to a dramatic increase of the transcriptional activity as compared with each single factor (95-fold, Fig. 4D), thus demonstrating a strong synergistic activity of the two TFs in regulating *Rnd2*. Surprisingly, transfection of an excess of *Tbr2* in respect to *Neurog2* caused a robust decrease in reporter activity as compared with the levels obtained using equimolar quantities of the two genes (Fig. 4D). This finding suggested that a tight regulation in the relative expression levels of the two factors is crucial for correct radial migration of young neurons emerging from the germinal zones of the developing cortex. To corroborate this hypothesis in vivo, the two TFs were electroporated alone or together in the E13.5 developing cortex. Surprisingly, pNeurod1-Tbr2 overexpression leads to radial migration deficits accompanied with a robust *Rnd2* expression decrease (Fig. 4A, E and F, Figure S4B). In contrast, concurrent overexpression of either *Rnd2* or *Neurog2* was sufficient to significantly rescue the block of cell migration caused by Tbr2 forced expression (Fig. 4E and F). In line with our in vivo data, genetic ablation of *Tbr2* increases the expression of this gene (Figure S4C, D). Altogether, these data demonstrate that TBR2 and NEUROG2 cooperate to regulate radial neuronal migration. Despite the complex cross-regulation established in the developing neurons, likely involving others cofactors to finely tune *Rnd2* gene activation and maintenance, the TBR2/NEUROG2 interaction appears to be crucial for the correct transcriptional control of this small GTP-binding protein.

Tbr2 Negatively Regulates the RGC-specific Rapid Proliferation Rate

We noted that a good number of putative TBR2 targets are known to regulate cell division and cell-cycle progression (Figure S1A). We therefore asked whether Tbr2 could have a role in neuronal progenitor proliferation. In fact, while RGCs divide repeatedly with short cell-cycle time, the INPs generally go through one cell division before irreversibly exiting cell-cycle. To investigate this issue, we overexpress *Tbr2* in proliferating NSCs (Conti and Cattaneo 2010) isolated from E14.5 embryonic cortices and maintained in vitro as adherent cultures. Acute *Tbr2* lentiviral transduction caused a robust decrease in NSC proliferation as scored by quantifying BrdU incorporation in cells after 2 h labeling (Fig. 5A, B). We then evaluated the expression of putative TBR2 targets as identified in ChIP-Seq analysis involved in cell-cycle control such as the Notch signaling effector protein *Hes5*, microcephalin 1 (*Mcph1*), Cdk5 regulatory subunit associated protein 2 (*Cdk5rap2*), *Btg2, Gadd45g* and cyclin dependent kinase inhibitor (*Cdkn1b*) (Fig. 5C). qPCR assays showed that Tbr2 overexpression caused a dramatic downregulation of *Hes5, Mcph1 and Cdkrap2* that are closely associated with cell-cycle progression. In contrast, those factors associated with cell-cycle arrest like *Btg2* and *Cdkn1b* were unchanged or moderately down-regulated (Fig. 5C). These results suggest that *Tbr2* can negatively modulate cell proliferation by controlling key molecules in this process. However, in vitro NSC proliferation dynamics differ significantly from the mitotic pattern observed in cortical INPs (Breunig et al. 2011). Thus, we moved in vivo to determine the fraction of cells in active cell-cycle 24 h after *Tbr2* electroporation (Figure S5B). Differently from previous findings on in vitro cultures, the fraction of GFP^+ cells that display Ki67 positivity remained unchanged upon *Tbr2* overexpression (Figures S5C, and S5D). To limit gene overexpression to the highly proliferative RGCs in the VZ, we examined the cells within 6 h after electroporation (Fig. 5D). At this early time point, Tbr2 targeted cells already expressed the exogenous protein (Figure S5A) and exhibited both a lower BrdU incorporation (1 h pulse) and a reduction in the number of Ki67 positive cells compared with controls (Fig. 5E–G).

To better investigate the discrepancy with the already reported proliferative induction of SVZ cells (Sessa et al. 2008), we analyzed gene expression exclusively in the electroporated cells by performing FACS-sorting of GFP+ cells followed by qPCR gene expression analysis 24 h after surgery (Fig. 5F). Validating the system, *Tbr2* was found highly expressed in the sorted *Tbr2*-iresGFP cell population while *Pax6* and *Sox2* resulted strongly down-regulated (Fig. 5H), suggesting a shift from RGCs to INP genetic program as previously reported

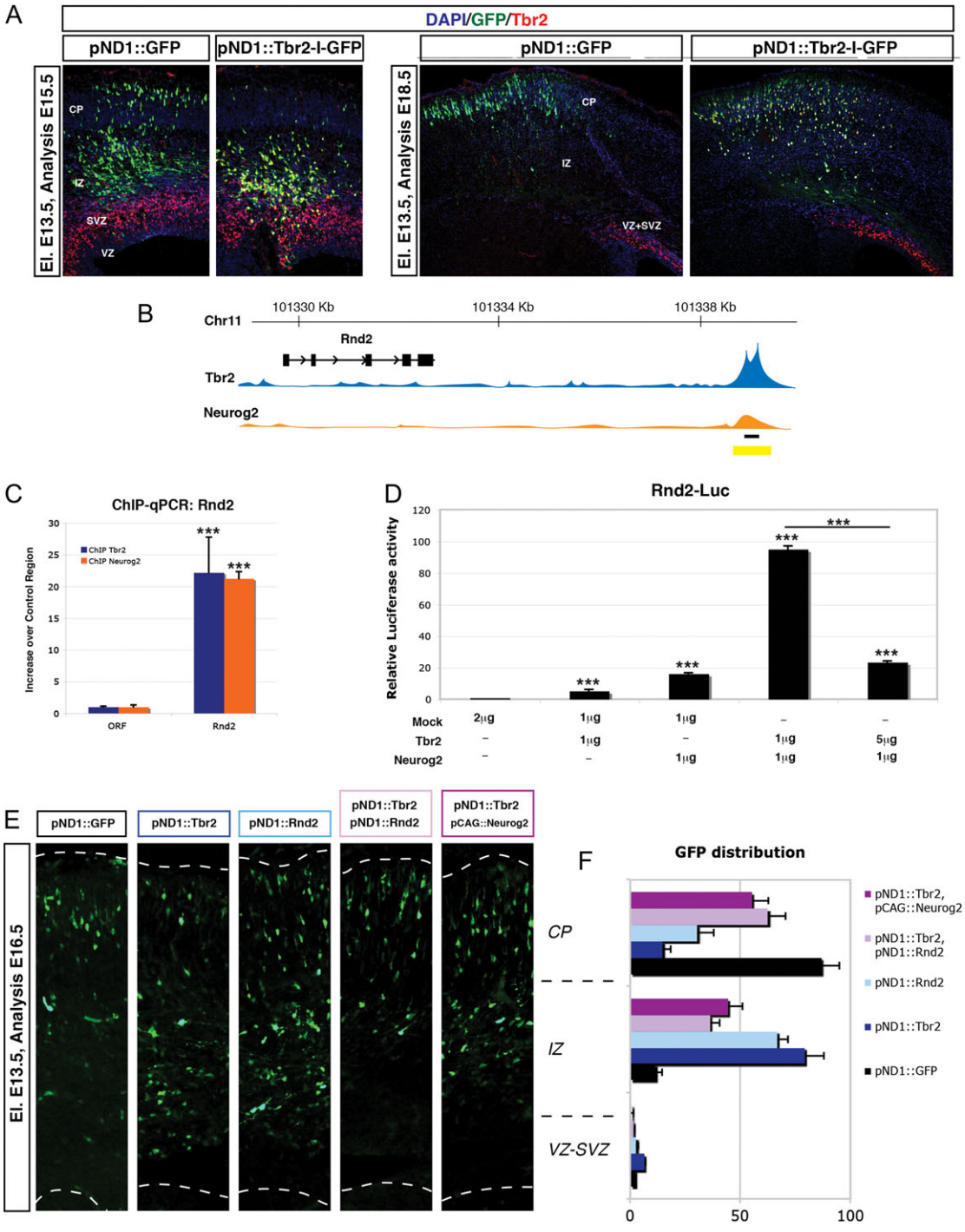

Figure 4. Tbr2 and Neurog2 control radial migration by modulating Rnd2 gene expression. (*A*) Forced expression via in utero electroporation of GFP (control) or Tbr2 and GFP regulated by the pNeurod1 promoter in E13.5 wild-type cortex and analyzed 2 days (left part) or 5 days (right part) after the surgery. Immunohistochemistry for GFP and TBR2 are reported. (*B*) Visualization of Tbr2 (blue track) and Neurog2 (orange track) ChIP-seq peaks in the Rnd2 genomic locus. (*C*) qPCR analysis on independent Tbr2 and Neurog2 ChIP samples for the region containing the Tbr2 and Neurog2 overlapping peaks in close proximity with the Rnd2 gene. ORF is negative control region. Quantification in triplicate from at least two immunoprecipitations. Mean ± SEM. (*D*) Luciferase assay using the same region tested in C using Tbr2, Neurog2 and the two TFs together both in 1:1 and 5:1 ratio. (*E*) Radial migration after 3dd from in utero electroporation of either pNeurod1::GFP (control) or pNeurod1::Tbr2-I-GFP, pNeurod1::Rnd2-I-GFP, pNeurod1::Tbr2-I-GFP, pNeurod1::Rnd2-I-GFP, pNeurod1::Tbr2-I-GFP or pCAG::Neurog2-I-GFP. GFP staining for each condition is reported. (*F*) Quantification of the cells migrated along the cortical wall after 3dd. Percentages of GFP cells in VZ-SVZ, inner zone (IZ) and CP are plotted for each condition. * = t-test, $P < 0.05$; *** = t-test, $P < 0.001$.

(Sessa et al. 2008). We then assessed the expression of the cell-cycle genes in the *Tbr2* electroporated cells. As previously found in vitro, *Hes5*, *Mcph1 and Cdk4rap2* were down-regulated (Fig. 5*I*), together with the increase of cyclin G2 (*Ccng2*) (data not shown) accounting for a negative impact on proliferation kinetics. However, the downregulation of *Btg2*, *Gadd45g* and *Cdkn1b* might restrain to exit from cell-cycle. To expand this analysis we evaluated the expression of the same genes after

acute *Tbr2* inactivation obtained by electroporating a Cre-expressing construct into the *Tbr2*$^{flox/flox}$ cortices. Forty-eight hours after acute *Tbr2* inactivation (a time requested to wash out the residual protein) expression of the RGC markers *Pax6* and *Sox2* was still retained (Fig. 5*H*), while genes promoting cell-cycle such as *Hes5*, *Cdk5rap2 and Cdkn1b* were found upregulated (Fig. 5*I* green bars) suggesting a scenario in which in the absence of Tbr2 the cells remained in a apical progenitor-

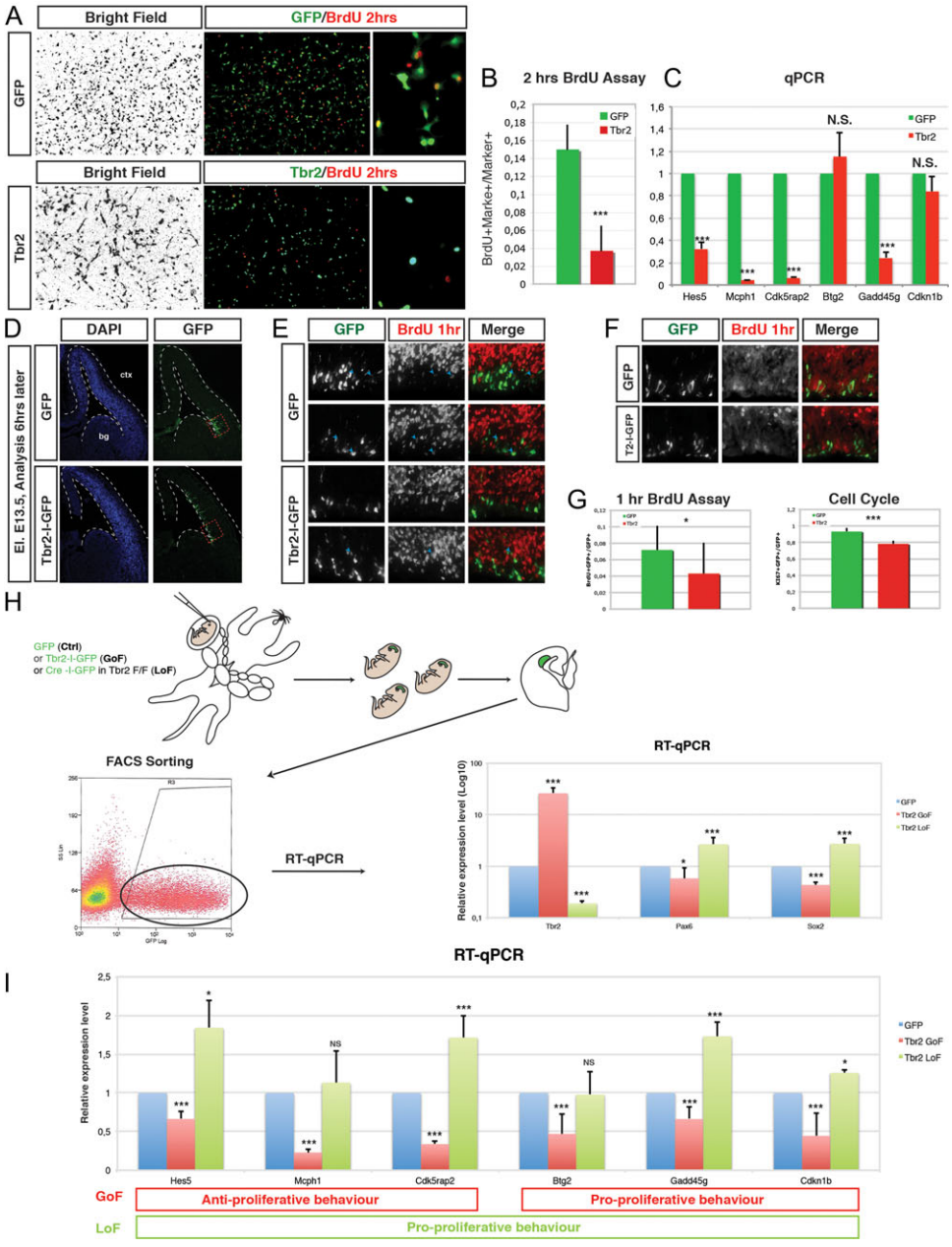

Figure 5. Tbr2 modulates cell-cycle dynamics of INPs in the developing cortex. (*A*) Adherent NSCs were infected with lentiviruses expressing GFP (control) or Tbr2 and assayed for BrdU incorporation (pulse of 2 h before fixation). Bright-field and immunohistochemistry for BrdU and GFP or Tbr2 are reported. (*B*) Quantification of the BrdU/GFP or BrdU/Tbr2 double positive cells on the total number of infected cells. (*C*) Expression of cell-cycle related genes Hes5, Mcph1, Cdk5rap2, Hes5, Ccng2, Btg2, Gadd45g and Cdkn1b by qPCR on NSCs infected with GFP or Tbr2. (*D*) Immunohistochemistry for GFP on coronal sections of E13.5 telencephali 6 h after in utero electroporation with either GFP (control) or Tbr2-I-GFP expression plasmids. (*E*) GFP and BrdU immunohistochemistry on cortical tissue 6 h after electroporation with GFP (control) or Tbr2 overexpressing contructs (magnification of the red boxed area in D). BrdU was pulsed 1 h before embryo isolation. (*F*) Immunohistochemistry for GFP and KI67 on cortical tissue 6 hours after electroporation with GFP (control) or Tbr2 overexpressing contructs (magnification of the red boxed area in A). (*G*) Quantification of dividing cells double positive for GFP and BrdU or KI67 on the total number of electroporated cells. (*H*) Schematic representation of the in utero electroporation experiments for Tbr2 overexpression (GoF) or acute ablation (LoF) in vivo. Wild-type embryos were electoporated with GFP (control) or Tbr2-I-GFP expression contructs and collected 24 h later. In addition, Tbr2$^{flox/flox}$ embryos were electroporated with GFP or Cre-I-GFP expression constructs and collected in the subsequent 48 h. GFP positive cortical patches were dissected out, dissociated and FACS-sorted to obtain a pure population of GFP^{+} cells. qPCR experiments confirm the upregulation of Tbr2 expression and concomitant downregulation of the RGC markers Pax6 and Sox2 in Tbr2 GoF and their upregulation in Tbr2 LoF. (*I*) Expression of cell-cycle related genes Hes5, Mcph1, Cdk5rap2, Btg2, Gadd45g and Cdkn1b by qPCR analysis upon Tbr2 gain or loss of function in vivo. * = t-test, $P < 0.05$; *** = t-test, $P < 0.001$; N.S. = t-test, $P > 0.05$.

like state. Altogether, these data define a cell type specific action of TBR2 on cell-cycle regulation. In fact, it counteracts cell proliferation in highly proliferating cells such as RGCs, as revealed on in vitro cultures of NSCs. However in less proliferating INPs, its action is permissive to cell-cycle progression, inhibiting the function of genes promoting cell-cycle arrest. These molecular findings provide a molecular understanding underlying the slow and limited proliferation behavior of the *Tbr2*$^+$ INPs (Noctor et al. 2004).

TBR2 Represses Neuronal Polarity and Neurite Outgrowth

During development, Tbr2 expression vanishes out exactly when INPs differentiate into mature cortical neurons. We, thus, asked whether maintaining Tbr2 expression beyond INP stage could interfere with neuronal morphological maturation. Remarkably, in vivo Tbr2 overexpression in cortical neurons caused a significant reduction in dendritic complexity as compared with control GFP expressing neurons, thus indicating a possible role for Tbr2 in preventing INPs to acquire a mature neuronal morphology (Figure S6A). To better investigate this effect we employed primary cultures of mouse embryonic hippocampal neurons. Upon isolation and subsequent plating in the dish, these neurons initially lack any neurite, but with time they mature in vitro developing a complex dendritic tree (Bradke and Dotti 2000). Two days in vitro (DIV) cultured hippocampal neurons were infected with GFP or *Tbr2*-GFP and the effects were tested 3 days afterwards on neurite development and branching (Figure S6B). Sholl analysis (Sholl 1953) showed that *Tbr2*$^+$ neurons exhibited an evident simplified morphology with reduced neurite branching compared with GFP+ only expressing neurons (Figure S6C). In addition, we noticed that crucial regulators of neurite outgrowth were included TBR2 target gene dataset and could therefore mediate this effect. Thus, we performed qPCR expression profiling of some of these candidates in FACS-isolated cells from cortical tissue electroporated with *Tbr2*-GFP after 48 h. Of note, we found that TBR2 was able to strongly repress the p21-activated kinases *Pak1* and *Pak3* (Hayashi et al. 2007; Nikolic 2008; Demyanenko et al. 2010), Rac GTP exchange factors *Tiam1* and *Tiam2* (Ehler et al. 1997; Miyamoto et al. 2006; Shirazi Fard et al. 2010; Goto et al. 2011; Demarco et al. 2012) and the microtubule associate protein-2 *Map2* (Harada et al. 2002) (Figure S6D). The same genes were similarly repressed in the *Tbr2* infected hippocampal neurons (data not shown). Conversely, *Tbr2* acute loss-of-function caused a reciprocal gene expression alteration with a heightened expression of these factors (Figure S6D, green bars). These findings suggest that TBR2 represses important determinants of neuronal polarity that promote axonal growth and dendritic complexity in developing cortical neurons, as for the case of the *Tiam* and *PAK* factors. Thus, the prevention of the neuronal morphological maturation of INPs represents a key role of TBR2 that together with its importance for resolution of RGC features are crucial for the maintenance of the correct cell shape of INPs while remaining in the SVZ domain.

TBR2 Interacts with JMJD3 for the Timely Activation of the Neuronal Specific Genes

Recent studies have revealed how the epigenetic control of gene transcription is pivotal to maintain the balance between RGC self-renewal and differentiation (Meaney and Ferguson-Smith 2010). In particular, the repressive epigenetic mark H3K27me3 induced by the Polycomb Repressive Complex is critical for the widespread repression of regulatory genes responsible for neuronal cell lineage determination (Boyer et al. 2006; Lee et al. 2006). We noticed that a significant fraction of the putative TBR2 binding domains were located into regulatory regions considerably enriched for the repressive histone mark H3K27me3 (Mohn et al. 2008), belonging to genes normally expressed in the developing cortical plate, e.g. *Tbr1, Cdh8, Cdh13, Camk2b* and others (Figure S7A and Table S1D). Interestingly, by comparing the TBR2 binding sites and the H3K27me3 enriched sequences we found common DNA regions associated to genes important for cortical development, e.g. *Slc17a6, Sox5, Bcl11b, Bhlhe22* (Figure S7B and Table S1E) (Ramos et al. 2013). Considering that the enrichment in H3K27me3 histone mark was found in promoters of neural progenitors, their associated genes were predicted to be activated during neuronal maturation by active demethylation (Figure S7C). Thus, we sought to investigate whether the activation of these genes during in vivo neuronal differentiation was associated to specific H3K27me3 demethylation. For this aim, we isolated by FACS the GFP$^-$ and GFP$^+$ cell populations from E14.5 *Tbr2*-GFP mouse cortices, which corresponded to RGCs/early INPs and late INPs/neurons, respectively (Kwon and Hadjantonakis 2007; Sessa et al. 2008) (Figure S7D). As expected, GFP$^+$ cells showed a robust decrease in the cell progenitor markers *Pax6* and *Ccnd2*, together with the upregulation of the neuronal differentiation-associated genes *Dcx, Mef2c, Tbr1, NeuroD1, Sox5* and others (Figure S7E). We then assessed the respective H3K27me3 levels by ChIP assay within the TBR2 binding regions associated with these genes. Intriguingly, we found a consistent reduction of this epigenetic mark in the majority of these regions in the GFP$^+$ compared with the GFP$^-$ cell populations (Figure S7F). To independently confirm these data, we performed a comparison between E14.5 versus E18.5 cortices, reasoning that at late developmental stages there is a drastic loss of cortical neural progenitors and an enrichment in postmitotic neurons. Accordingly, we confirmed an upregulation of the genes of interests at E18.5 (Figure S7G) that was accompanied with the H3K27me3 demethylation on the associated regulatory regions in a large fraction of these genes (Figure S7H). Altogether, these data demonstrate that the majority of the TBR2 putative target genes transcriptionally upregulated during neuronal differentiation are subjected to H3K27 demethylation during cortical development.

It has been recently shown that T-box protein-dependent transcriptional activation can be mediated by JMJD3 and UTX demethylases during immune system differentiation (Miller et al. 2008, 2010). Thus we asked whether TBR2 can interact with histone demethylase(s) in the neural cells and thereby promote neuronal gene activation. While *Utx* is not expressed in the developing brain (data not shown), *Jmjd3* transcripts were detected in virtually all the cell types of the developing cortex including the *Tbr2*$^+$ progenitors (Fig. 6A–C). Interestingly, we noticed that a fraction of the TBR2 binding regions were shared with those targeted by JMJD3 in NSCs (Estaras et al. 2012) and, among them, those associated with genes expressed in the cortical plate, e.g. *Satb2, Sox5, Tle4, Hdac5* (Fig. 6D and Table S1F). GO biological processes enriched in this intersection were consistent with cortical development (Fig. 6E and Table S2D). Notably the overlapping regions between TBR2 and JMJD3 were distributed in the genome similarly to the whole TBR2 dataset while they differed from the entire set of JMJD3 targets that resulted more associated to gene promoters (Fig. 6F) (Estaras et al. 2012). Thus, we sought to test whether

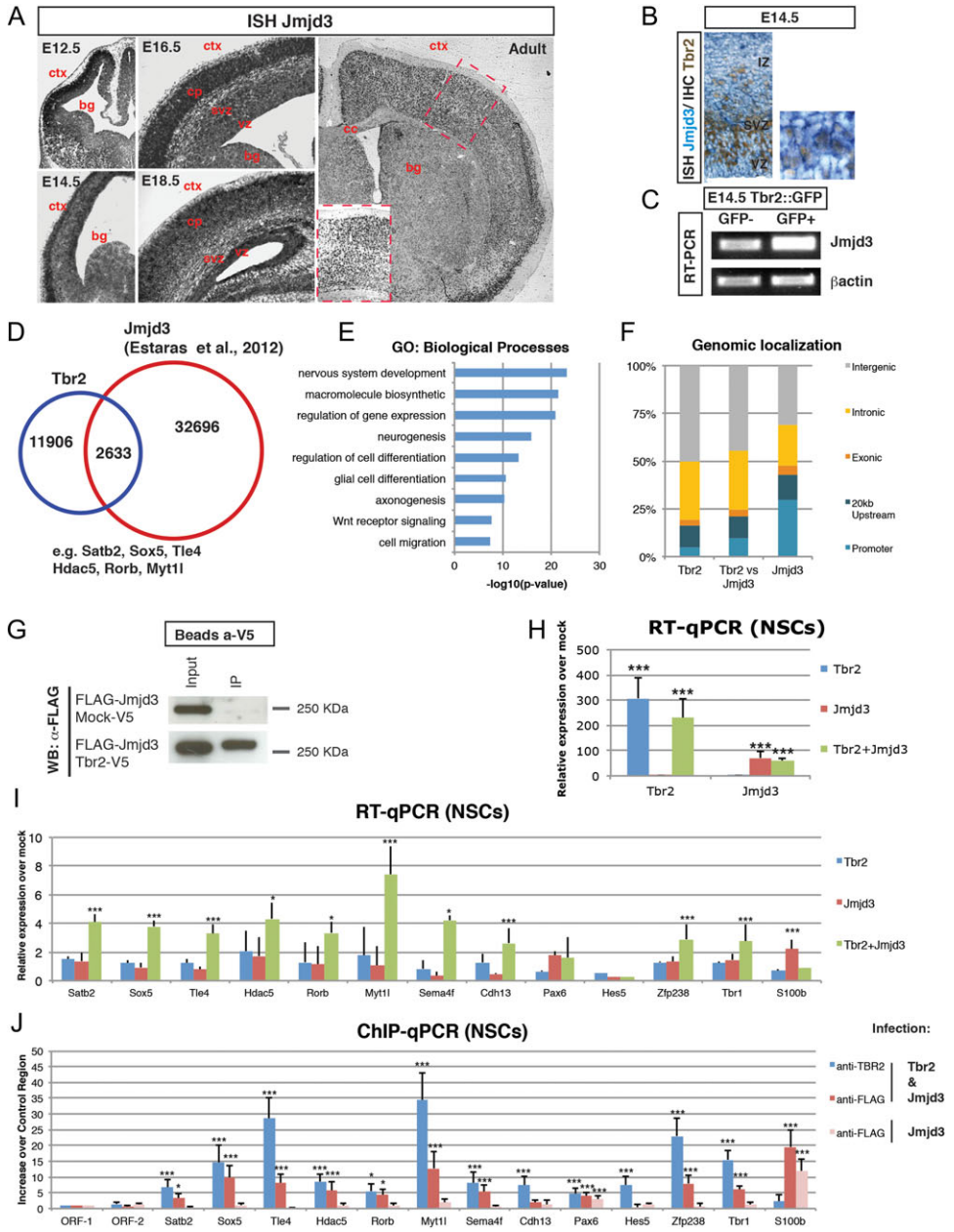

Figure 6. TBR2 associates and functionally interacts with JMJD3. (*A*) Jmjd3 expression pattern during cortical development and in the adult forebrain by in situ hybridization. (*B*) Tbr2 protein localization (immunohistochemistry) coupled to Jmjd3 gene expression pattern (RNA in situ hybridization) showing colocalization in the cortical SVZ domain. (*C*) Semi-quantitative PCR for Jmjd3 and β-actin (as normalizer) in GFP^- and GFP^+ cell fraction isolated from cortical tissue of pTbr2::GFP transgenic mice. (*D*) Venn diagram showing the overlap between Tbr2 (blue) and Jmjd3 (red) peaks in neural precursors in vitro. (*E*) Enrichment of GO biological process terms in genes associated (the nearest TSS) with the regions shared by Tbr2 and Jmjd3 ChIP-seq. (*F*) Graph illustrating the genomic location of ChIP-Seq peaks for Tbr2, Jmjd3 and the intersection between them. (*G*) Coimmunoprecipitation using anti-V5 antibody performed in whole protein extracts from NSCs infected with FLAG-Jmjd3 and either mock-V5 or Tbr2-V5 vector revealing the presence of JMJD3 and TBR2 in the same physical complex. (*H*) Tbr2 and Jmjd3 expression in NSCs infected with either Tbr2 or Jmjd3 or both over mock treated cells. (*I*) Expression levels of the genes coregulated by the two factors Tbr1, Satb2, Zfp238, Sox5, Tle4, the Jmjd3 regulated gene S100b and the RGC markers Hes5 and Pax6. (*J*) Enrichment analysis by qPCRs on ChIP samples obtained either with anti-Tbr2 (blue bars) or anti-FLAG antibodies (red bars) for TBR2 target regions in NSCs coinfected with Tbr2 and Jmjd3-FLAG or with anti-FLAG antibody in NSCs infected only with Jmjd3-FLAG (pink bars). Quantification in triplicate from at least two ChIP experiments. Mean ± SEM. * = t-test, $P < 0.05$; *** = t-test, $P < 0.001$; N.S. = t-test, $P > 0.05$. cc = corpus callosum.

TBR2 and JMJD3 can interact physically and functionally. Remarkably, TBR2 and JMJD3 can be associated within the same protein complex as shown in coimmunoprecitipation experiments on NSC extracts (Fig. 6G). To test any functional interaction between these two proteins, we compared the expression of candidate genes in proliferating NSCs overexpressing *Tbr2*, *Jmjd3* or the two factors together (Fig. 6H). Remarkably, expression of neuronal-specific genes like *Sox5*, *Tle4*, *Zfp238* and others resulted strongly upregulated only when both *Tbr2* and *Jmjd3* were coexpressed. (Fig. 6I). Of note, this was not the case for either NSC specific genes *Hes5* and *Pax6* or the known JMJD3 target astroglial related gene *S100b*, which was activated only by the *Jmjd3* overexpression (Fig. 6I). We then performed independent ChIP-qPCRs for TBR2 and

JMJD3 on NSCs coexpressing both exogenous genes. These experiments revealed a robust enrichment of both proteins on the regulatory regions of the overexpressed genes (Fig. 6J). However, when NSCs were infected with JMJD3 alone, its binding was not detectable on the TBR2 coregulated targets, while it was still maintained on the *S100b* gene locus (Fig. 6J). Altogether, these results reveal that removing the H3K27me3 repressive mark through the combinatorial action of TBR2 and JMJD3 activates some critical determinants of the cortical neuronal differentiation.

To validate the relevance of this mechanism in vivo, we employed the in utero electroporation system to target the developing cortex with plasmids expressing *Tbr2* and/or a negative form of *Jmjd3* in which the catalytic JmjC domain is inactivated (*Jmjd3*-Mut) (Burgold et al. 2008) (Figure S8). Forty-eight hours after surgery, electroporated control cells were partially migrated along the cortical plate (Figure S8A), while the cells expressing *Tbr2* and *Jmjd3*-Mut (alone or in combination) were arrested in the SVZ region (Figures S8B, S8C and S8D). We then FACS-sorted the GFP$^+$ cells from cortices electroporated with the different gene combinations and investigate the expression levels of the candidate genes by qPCR (Figure S8E and S8F). Although misexpression of *Tbr2* alone was sufficient to robustly up-regulate candidate neuronal specific genes (Figure S8F, blue bars), coexpression with the *Jmjd3*-Mut strongly repressed the TBR2-mediated activation on the majority its target genes (Figure S8F, green bars). These data suggests that TBR2 requires the catalytic activity of JMJD3 to de-repress a set of its specific targets.

We then wondered whether full inactivation of *Jmjd3* in mice would lead to defects in cerebral cortex development resembling those described for *Tbr2* loss of function. Since *Jmjd3* knock-out mice die at birth we therefore limited our analysis to embryonic stages (Satoh et al. 2010). E18.5 *Jmjd3* mutants exhibited a microcephalic phenotype with a significant thinner cortical wall (Fig. 7A). As previously reported for *Tbr2* gene inactivation (Arnold et al. 2008; Sessa et al. 2008), *Jmjd3* mutants exhibited a significant reduction in the SATB2$^+$

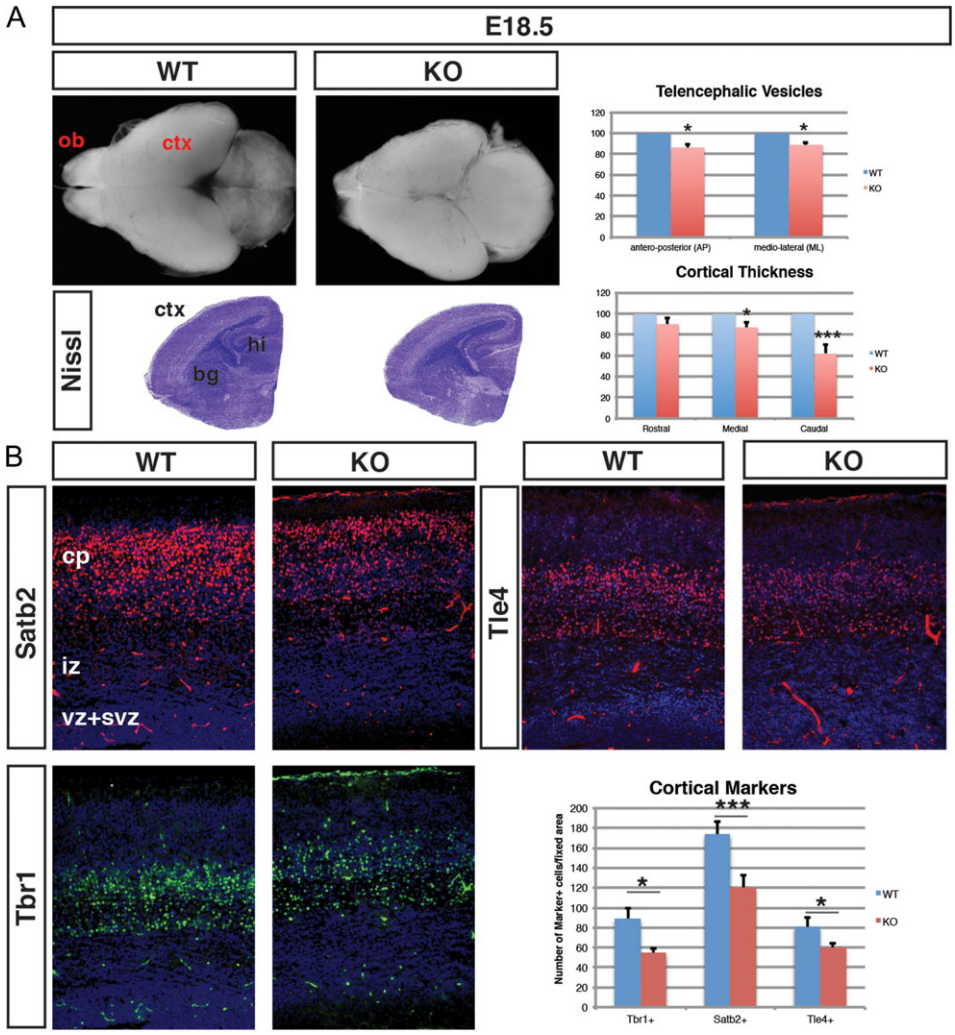

Figure 7. Jmjd3 and Tbr2 mutant cortices display related morphological defects. (A) Low magnification view and Nissl staining of sagittal sections of wild-type and Jmjd3 mutant cortices at E18.5. Graphs illustrating relative size of telencephalic vescicle antero-posterior and medio-lateral axes (up) and of cortical thickness at rostral, medial and caudal levels (bottom) of Jmjd3 mutant (red bars) and relative control (blue bar) cortices. (B) E18.5 wild-type and Jmjd3 mutant cortices immunostained for the upper-layers marker SATB2 and the deeper-layers markers TLE4 and TBR1. Quantifications of the three markers in wild-type (blue bar) and Jmjd3 mutant (red bars) cortices. (C) Expression patterns of *Sox5*, *Tle4* and *Math2* in Jmjd3 and Tbr2 mutant and relative control cortices at E14.5. Higher magnifications of the cortical domains are presented in insets. ob = olfactory bulbs, hi = hippocampus. * = t-test, $P < 0.05$; *** = t-test, $P < 0.001$.

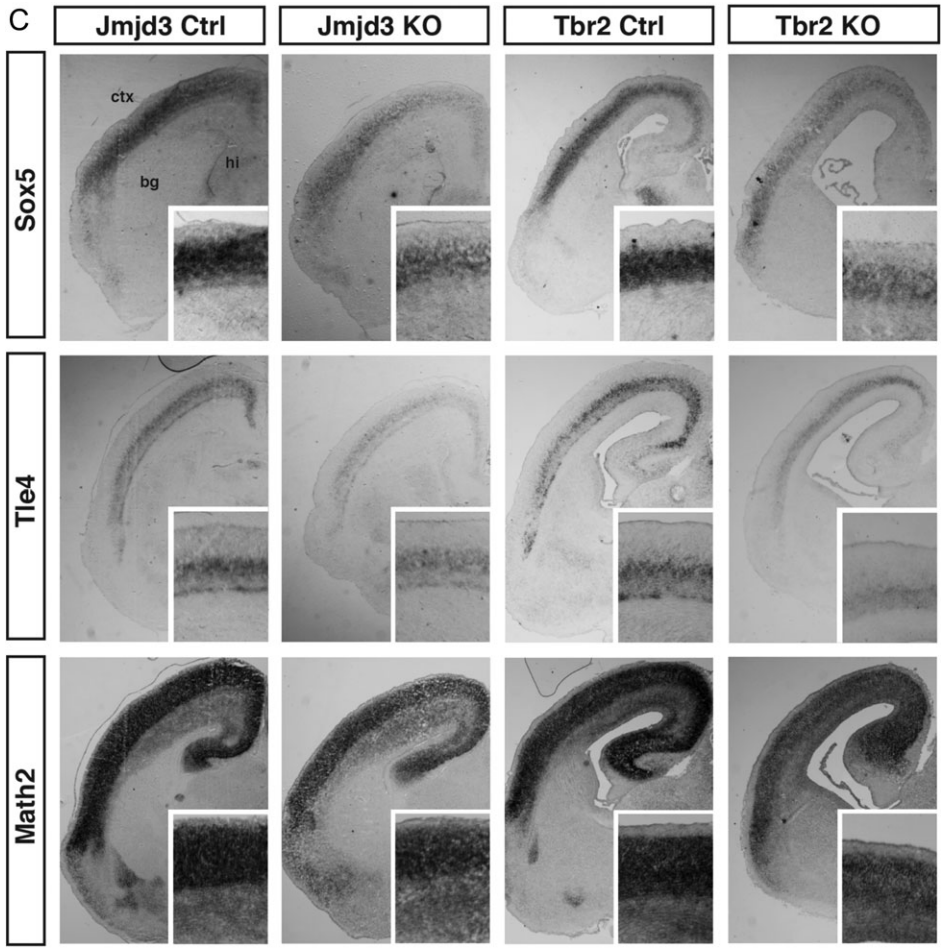

Figure 7. *Continued.*

and TBR1^{+}/TLE4^{+} neuronal populations defining the upper and cortical layers, respectively (Fig. 7*B* and data not shown). Likewise, gene expression pattern of additional markers of layer identity such as *Sox5, Tle4 and Math2* revealed a similar reduced expression domain confirming the general loss of cortical neurons in *Jmjd3* mutants (Fig. 7*C*). This analysis confirms the critical role of JMJD3 in cortical development that might be related to its function in activating critical genes in neuronal differentiation in cooperation with TBR2. Again, both *Tbr2* and *Jmjd3* gene inactivation lead to a comparable reduction in cerebral cortex growth leading to microcephaly with comparable neuronal loss in both deep and superficial cortical layers.

Altogether these data strongly suggest that TBR2 and JMJD3 act synergistically to promote neuronal differentiation, by acting together on a subset of their respective molecular targets. Mechanistically, TBR2 might direct JMJD3 on its target gene regulatory regions to erase the H3K27me3 repressive mark by active demethylase activity and thus by de-repressing the neuronal lineage specific genes maintained in a poised or bivalent state in neural progenitors (Mohn et al. 2008; Hirabayashi and Gotoh 2010).

Discussion

In this study, we uncovered the molecular network regulated by *Tbr2* during cortical development. This was obtained by combining transcriptome profiling of *Tbr2* mutant cortices together with in vivo analysis of TBR2 binding sites at whole genome scale. Our results demonstrate that *Tbr2* is a master regulator of INP identity by controlling an array of molecular pathways responsible for both INP progression along the glutammatergic lineage and blocking of alternative neural fates. In particular, we have defined the critical TBR2 target genes having an impact on the fundamental aspects of INPs such as cell-cycle profile, morphology, migration and glutammatergic lineage cell fate. Importantly, this study identified a genetic and an epigenetic cofactor with a major role in controlling TBR2 transcriptional activity. In fact, our data demonstrated that TBR2 can act as a molecular partner with NEUROG2 for transcriptional regulation during corticogenesis, not just as a NEUROG2 downstream effector as showed previously (Kovach et al. 2013). We revealed a possible example of the TBR2/NEUROG2 combinatorial action involved in the precise modulation of *Rnd2*, a gene with a fundamental role in cortical neural radial migration modulating RhoA signaling (Heng et al. 2008; Pacary et al. 2011). An unexpected complexity in the modulation of *Rnd2* expression depending on the relative dosage of TBR2 and NEUROG2 has been highlighted. We privilege a model in which, equal levels of these two factors are able to sustain the highest *Rnd2* expression that occurs in a very specific phase of INPs, coinciding with the initiation of their radial migration while exiting the SVZ. The absence of Tbr2 – probably scrambling the correct sequence of events occurring in

glutammatergic development – promotes precocious radial migration, which dependents on high level of *Rnd2* as shown herein (Figure S5). Considering the high number of bound regions shared by TBR2 and NEUROG2, we predict that their combinatorial functions are likely operating on other important target genes (Fig. 3). This scenario would explain why relatively few factors are regulating a wide array of cellular behaviors during cortical neuronal differentiation and it is in line with the fast dynamics of Neurogenin1/2 expression levels that can alter the relative ratio between NEUROG2 and TBR2 levels (Shimojo et al. 2008; Wilkinson et al. 2013). This combinatorial activity with different outputs, based on the two factor relative ratio, offers a fast and flexible mechanism for the fine control of the excitatory neuronal specification and migration in the developing cortex.

In this study, we also identified the histone demethylase JMJD3/KDM6B as the first epigenetic regulator directly associated with TBR2. This is of particular interest, since we provided first evidence that an active mechanism of H3K27me3 demethylation via the TBR2/JMJD3 protein cooperation is required for priming the activity of genes specific for the glutammatergic neuronal lineage determination and differentiation. Recently, it has been shown that JMJD3 can be recruited on both promoters and enhancers of genes relevant for neuronal and cortical development, and its activity is necessary for correct neuronal differentiation (Park et al. 2014). However, how JMJD3 is recruited to its correct targets in a cell-type and stage specific manner is largely unknown (Fig. 6A–C). It has been showed that JMJD3 activity is essential for TGFβ-induced neuronal differentiation and its interaction with SMAD3 on a set of downstream promoters (Estaras et al. 2012). Similarly, the tumor-suppressor P53 can interact with JMJD3 to modulate neurogenesis (Sola et al. 2011). Finally, the JMJD3 binding to MLL1, a component of the trithorax group remodeling complex, leads to activation of specific target genes, including the neurogenic determinant *Dlx2* during adult neurogenesis (De Santa et al. 2007; Park et al. 2014). Moreover, the association between JMJD3 and the T-box factors is crucial for the correct T cell function (Miller 2008, 2010) and endoderm differentiation (Kartikasari et al. 2013), but this interaction has never been studied in cerebral cortex development where T-box factors have a significant role (Hevner et al. 2006). Intriguingly, TBR2 is capable of recruiting JMJD3 thus spatially and temporally restricting its action on specific enhancers in the INP stage, a transient but critical step in cortical excitatory neuronal cell fate acquisition. This mechanism can account for the epigenetic silencing of a cohort of developmentally regulated genes during the neural progenitor stage, a chromatin modification to keep them silenced but ready for activation, to prime their full expression in postmitotic neurons. In addition, this molecular system might explain the aberrant expression of a subset of genes like *Ebf1/2/3* and *Gbx2* as caused by the uncontrolled action of JMJD3 on its non-cortical specific target genes. On this line, the TBR2/JMJD3 interaction would contribute to the simultaneous activation of the specific transcriptional program responsible for the neurogenic process as well as to the silencing of alternative gene expression networks.

Although from our data we cannot infer a specific mechanism of action for the TBR2/JMJD3 complex, Kartikasari et al. (2013) suggested that during definitive endoderm cell lineage differentiation the two proteins control gene expression by regulating the spatial reorganization of large chromatin domains to allow coherent enhancer-promoter interactions (Kartikasari et al. 2013). On the same line, during neuronal differentiation TBR2/JMJD3 might promote a specific chromatin architecture that would facilitate the activation of genetic determinants for this process. These findings provide support and validation in vivo of previous results performed exclusively in vitro about the correct neuronal cell differentiation regulated by epigenetic mechanisms (Mikkelsen et al. 2008; Mohn et al. 2008; Hirabayashi and Gotoh 2010). Of note, a significant set of TBR2 binding regions does not appear to have an evident enriched H3K27me3 profile. These results depend from the fact that the available datasets have been extracted from heterogeneous experimental settings and different tissues/regions therefore limiting the informative value of this comparative analysis. Thus, future assessment of the H3K27 methylation dynamics over different stages in the developing cortex and its different cell types will provide the ground to match the epigenetic changes with the action of the developmental transcription factors involved in these processes.

Translating these results from mouse to human can be hard due to the different kinetics of the involved transcription factors during the different steps of corticogenesis in the two species. For instance, Pax6 and Tbr2 are rarely present in the same cells in mice, while they are largely coexpressed at in human OSVZ progenitors. Thus, while the downstream targets can differ in a species-specific manner, our results can help to explore the peculiarities that are crucial for cerebral cortex development and glutammatergic neuronal specification. In conclusion, this study defines *Tbr2* as a critical regulator for INPs by controlling a large and complex genetic network responsible for multiple aspects of the biology of this particular class of neuronal progenitors.

Supplementary Material

Supplementary material can be found at: http://www.cercor.oxfordjournals.org/.

Funding

European Research Council (AdERC #340527), Telethon grants (GGP15096, GGP11110) and the Italian Ministry of Health (Young investigator grant # GR-2013-02355540).

Notes

We thank L. Muzio, R. Galli, D. Castro, R. Hevner, G. Testa, Yong Chao Ma and Mike Greenberg for helpful discussion and sharing of reagents. *Conflict of Interest*: Nonedeclared.

References

Arnold SJ, Huang GJ, Cheung AF, Era T, Nishikawa S, Bikoff EK, Molnár Z, Robertson EJ, Groszer M. 2008. The T-box transcription factor Eomes/Tbr2 regulates neurogenesis in the cortical subventricular zone. Genes Dev. 22:2479–2484.

Asami M, Pilz GA, Ninkovic J, Godinho L, Schroeder T, Huttner WB, Götz M. 2011. The role of Pax6 in regulating the orientation and mode of cell division of progenitors in the mouse cerebral cortex. Development. 138:5067–5078.

Ayala R, Shu T, Tsai LH. 2007. Trekking across the brain: the journey of neuronal migration. Cell. 128:29–43.

Baala L, Briault S, Etchevers HC, Laumonnier F, Natiq A, Amiel J, Boddaert N, Picard C, Sbiti A, Asermouh A, et al. 2007. Homozygous silencing of T-box transcription factor EOMES leads to microcephaly with polymicrogyria and corpus callosum agenesis. Nat Genet. 39:454–456.

Bertrand N, Castro DS, Guillemot F. 2002. Proneural genes and the specification of neural cell types. Nat Rev Neurosci. 3: 517–530.

Boyer LA, Plath K, Zeitlinger J, Brambrink T, Medeiros LA, Lee TI, Levine SS, Wernig M, Tajonar A, Ray MK, et al. 2006. Polycomb complexes repress developmental regulators in murine embryonic stem cells. Nature. 441(7091):349–353.

Bradke F, Dotti CG. 2000. Establishment of neuronal polarity: lessons from cultured hippocampal neurons. Curr Opin Neurobiol. 10(5):574–581.

Breunig JJ, Haydar TF, Rakic P. 2011. Neural stem cells: historical perspective and future prospects. Neuron. 70(4):614–625.

Burgold T, Spreafico F, De Santa F, Totaro MG, Prosperini E, Natoli G, Testa G. 2008. The histone H3 lysine 27-specific demethylase Jmjd3 is required for neural commitment. PLoS One. 3:e3034.

Castro DS, Martynoga B, Parras C, Ramesh V, Pacary E, Johnston C, Drechsel D, Lebel-Potter M, Garcia LG, Hunt C, et al. 2011. A novel function of the proneural factor Ascl1 in progenitor proliferation identified by genome-wide characterization of its targets. Genes Dev. 25(9):930–945.

Colombo E, Galli R, Cossu G, Gecz J, Broccoli V. 2004. Mouse orthologue of ARX, a gene mutated in several X-linked forms of mental retardation and epilepsy, is a marker of adult neural stem cells and forebrain GABAergic neurons. Dev Dyn. 231:631–639.

Conti L, Cattaneo E. 2010. Neural stem cell systems: physiological players or in vitro entities? Nat Rev Neurosci. 11(3):176–187.

de Juan Romero C, Bruder C, Tomasello U, Sanz-Anquela JM, Borrell V. 2015. Discrete domains of gene expression in germinal layers distinguish the development of gyrencephaly. EMBO J. 34(14):1859–1874.

De Santa F, Totaro MG, Prosperini E, Notarbartolo S, Testa G, Natoli G. 2007. The histone H3 lysine-27 demethylase Jmjd3 links inflammation to inhibition of polycomb-mediated gene silencing. Cell. 130:1083–1094.

Demarco RS, Struckhoff EC, Lundquist EA. 2012. The Rac GTP exchange factor TIAM-1 acts with CDC-42 and the guidance receptor UNC-40/DCC in neuronal protrusion and axon guidance. PLoS Genet. 8(4):e1002665.

Demyanenko GP, Halberstadt AI, Rao RS, Maness PF. 2010. CHL1 cooperates with PAK1-3 to regulate morphological differentiation of embryonic cortical neurons. Neuroscience. 165(1): 107–115.

Edgar R, Domrachev M, Lash AE. 2002. Gene Expression Omnibus: NCBI gene expression and hybridization array data repository. Nucleic Acids Res. 30:207–210.

Ehler E, van Leeuwen F, Collard JG, Salinas PC. 1997. Expression of Tiam-1 in the developing brain suggests a role for the Tiam-1-Rac signaling pathway in cell migration and neurite outgrowth. Mol Cell Neurosci. 9(1):1–12.

Elsen GE, Hodge RD, Bedogni F, Daza RA, Nelson BR, Shiba N, Reiner SL, Hevner RF. 2013. The protomap is propagated to cortical plate neurons through an Eomes-dependent intermediate map. Proc Natl Acad Sci USA. 110:4081–4086.

Estaras C, Akizu N, Garcia A, Beltran S, de la Cruz X, Martınez-Balbas MA. 2012. Genome-wide analysis reveals that Smad3 and JMJD3 HDM co-activate the neural developmental program. Development. 139:2681–2691.

Fietz SA, Kelava I, Vogt J, Wilsch-Bräuninger M, Stenzel D, Fish JL, Corbeil D, Riehn A, Distler W, Nitsch R, et al. 2010. OSVZ progenitors of human and ferret neocortex are epithelial-like and expand by integrin signaling. Nat Neurosci. 13(6):690–699.

Florio M, Albert M, Taverna E, Namba T, Brandl H, Lewitus E, Haffner C, Sykes A, Wong FK, Peters J, et al. 2015. Human-specific gene ARHGAP11B promotes basal progenitor amplification and neocortex expansion. Science. 347(6229):1465–1470.

Fode C, Ma Q, Casarosa S, Ang SL, Anderson DJ, Guillemot F. 2000. A role for neural determination genes in specifying the dorsoventral identity of telencephalic neurons. Genes Dev. 14:67–80.

Gal JS, Morozov YM, Ayoub AE, Chatterjee M, Rakic P, Haydar TF. 2006. Molecular and morphological heterogeneity of neural precursors in the mouse neocortical proliferative zones. J Neurosci. 26:1045–1056.

Gentleman RC, Carey VJ, Bates DM, Bolstad B, Dettling M, Dudoit S, Ellis B, Gautier L, Ge Y, Gentry J, et al. 2004. Bioconductor: open software development for computational biology and bioinformatics. Genome Biol. 5(10):R80.

Goto A, Hoshino M, Matsuda M, Nakamura T. 2011. Phosphorylation of STEF/Tiam2 by protein kinase A is critical for Rac1 activation and neurite outgrowth in dibutyryl cAMP-treated PC12D cells. Mol Biol Cell. 22(10):1780–1790.

Götz M, Huttner WB. 2005. The cell biology of neurogenesis. Nat Rev Mol Cell Biol. 10:777–788.

Halbritter F, Kousa AI, Tomlinson SR. 2014. GeneProf data: a resource of curated, integrated and reusable high-throughput genomics experiments. Nucleic Acids Res. 42:D851–D858.

Halbritter F, Vaidya HJ, Tomlinson SR. 2012. GeneProf: analysis of high-throughput sequencing experiments. Nat Methods. 9:7–8.

Hansen DV, Lui JH, Parker PR, Kriegstein AR. 2010. Neurogenic radial glia in the outer subventricular zone of human neocortex. Nature. 464(7288):554–561.

Harada A, Teng J, Takei Y, Oguchi K, Hirokawa N. 2002. MAP2 is required for dendrite elongation, PKA anchoring in dendrites, and proper PKA signal transduction. J Cell Biol. 158(3): 541–549.

Hayashi K, Ohshima T, Hashimoto M, Mikoshiba K. 2007. Pak1 regulates dendritic branching and spine formation. Dev Neurobiol. 67(5):655–669.

Hébert JM, McConnell SK. 2000. Targeting of cre to the Foxg1 (BF-1) locus mediates loxP recombination in the telencephalon and other developing head structures. Dev Biol. 222: 296–306.

Heng JI, Nguyen L, Castro DS, Zimmer C, Wildner H, Armant O, Skowronska-Krawczyk D, Bedogni F, Matter JM, Hevner R, et al. 2008. Neurogenin 2 controls cortical neuron migration through regu- lation of Rnd2. Nature. 455:114–118.

Hevner RF, Hodge RD, Daza RA, Englund C. 2006. Transcription factors in glutammatergic neurogenesis: conserved programs in neocortex, cerebellum, and adult hippocampus. Neurosci Res. 55:223–233.

Hirabayashi Y, Gotoh Y. 2010. Epigenetic control of neural precursor cell fate during development. Nat Rev Neurosci. 11(6): 377–388.

Hodge RD, Nelson BR, Kahoud RJ, Yang R, Mussar KE, Reiner SL, Hevner RF. 2012. Tbr2 is essential for hippocampal lineage progression from neural stem cells to intermediate progenitors and neurons. J Neurosci. 18:6275–6287.

Huang HP, Liu M, El-Hodiri HM, Chu K, Jamrich M, Tsai MJ. 2000. Regulation of the pancreatic islet-specific gene BETA2 (neuroD) by neurogenin 3. Mol Cell Biol. 20:3292–3307.

Huang DW, Sherman BT, Lempicki RA. 2009. Systematic and integrative analysis of large gene lists using DAVID Bioinformatics Resources. Nat Protoc. 4(1):44–57.

Kahoud RJ, Elsen GE, Hevner RF, Hodge RD. 2014. Conditional ablation of Tbr2 results in abnormal development of the olfactory bulbs and subventricular zone-rostral migratory stream. Dev Dyn. 3:440–450.

Kartikasari AE, Zhou JX, Kanji MS, Chan DN, Sinha A, Grapin-Botton A, Magnuson MA, Lowry WE, Bhushan A. 2013. The histone demethylase Jmjd3 sequentially associates with the transcription factors Tbx3 and Eomes to drive endoderm differentiation. EMBO J. 32:1393–1408.

Konno D, Shioi G, Shitamukai A, Mori A, Kiyonari H, Miyata T, Matsuzaki F. 2008. Neuroepithelial progenitors undergo LGN-dependent planar divisions to maintain self-renewability during mammalian neurogenesis. Nat Cell Biol. 10:93–101.

Kovach C, Dixit R, Li S, Mattar P, Wilkinson G, Elsen GE, Kurrasch DM, Hevner RF, Schuurmans C. 2013. Neurog2 simultaneously activates and represses alternative gene expression programs in the developing neocortex. Cereb Cortex. 8: 1884–1900.

Kowalczyk T, Pontious A, Englund C, Daza RAM, Bedogni F, Hodge R, Attardo A, Bell C, Huttner WB, Hevner RF. 2009. Intermediate neuronal progenitors (basal progenitors) produce pyramidal-projection neurons for all layers of cerebral cortex. Cereb Cortex. 19:2439–2450.

Kwon GS, Hadjantonakis AK. 2007. Eomes:GFP-a tool for live imaging cells of the trophoblast, primitive streak, and telencephalon in the mouse embryo. Genesis. 45:208–217.

Lee TI, Jenner RG, Boyer LA, Guenther MG, Levine SS, Kumar RM, Chevalier B, Johnstone SE, Cole MF, Isono K, et al. 2006. Control of developmental regulators by polycomb in human embryonic stem cells. Cell. 125(2):301–313.

Mao CA, Kiyama T, Fururta Y, Hadjantonakis AK, Klein WH. 2008. Eomesodermin, a target gene of Pou4f2, is required for retinal ganglion cell and optic nerve development in the mouse. Development. 135:271–280.

Martínez-Cerdeño V, Cunningham CL, Camacho J, Keiter JA, Ariza J, Lovern M, Noctor SC. 2016. Evolutionary origin of Tbr2-expressing precursor cells and the subventricular zone in the developing cortex. J Comp Neurol. 524(3):433–447.

McLean CY, Bristor D, Hiller M, Clarke SL, Schaar BT, Lowe CB, Wenger AM, Bejerano G. 2010. GREAT improves functional interpretation of cis-regulatory regions. Nat Biotechnol. 28: 495–501.

Meaney MJ, Ferguson-Smith AC. 2010. Epigenetic regulation of the neural transcriptome: the meaning of the marks. Nat Neurosci. 13(11):1313–1318.

Mikkelsen TS, Hanna J, Zhang X, Ku M, Wernig M, Schorderet P, Bernstein BE, Jaenisch R, Lander ES, Meissner A. 2008. Dissecting direct reprogramming through integrative genomic analysis. Nature. 454:49–55.

Miller SA, Huang AC, Miazgowicz MM, Brassil MM, Weinmann AS. 2008. Coordinated but physically separable interaction with H3K27-demethylase and H3K4-methyltransferase activities are required for T-box protein-mediated activation of developmental gene expression. Genes Dev. 22(21):2980–2993.

Miller SA, Mohn SE, Weinmann AS. 2010. Jmjd3 and UTX play a de- methylase-independent role in chromatin remodeling to regulate T-box family member-dependent gene expression. Mol Cell. 40:594–605.

Miyamoto Y, Yamauchi J, Tanoue A, Wu C, Mobley WC. 2006. TrkB binds and tyrosine-phosphorylates Tiam1, leading to activation of Rac1 and induction of changes in cellular morphology. Proc Natl Acad Sci USA. 103(27):10444–10449.

Miyoshi G, Fishell G. 2012. Dynamic FoxG1 expression coordinates the integration of multipolar pyramidal neuron precursors into the cortical plate. Neuron. 74:1045–1058.

Mohn F, Weber M, Rebhan M, Roloff TC, Richter J, Stadler MB, Bibel M, Schübeler D. 2008. Lineage-specific polycomb targets and de novo DNA methylation define restriction and potential of neuronal progenitors. Mol Cell. 30:755–766.

Muzio L, DiBenedetto B, Stoykova A, Boncinelli E, Gruss P, Mallamaci A. 2002. Emx2 and Pax6 control regionalization of the pre- neuronogenic cortical primordium. Cereb Cortex. 12:129–139.

Naiche LA, Harrelson Z, Kelly RG, Papaioannou VE. 2005. T-box genes in vertebrate development. Annu Rev Genet. 39: 219–239.

Nikolic M. 2008. The Pak1 kinase: an important regulator of neuronal morphology and function in the developing forebrain. Mol Neurobiol. 37(2–3):187–202.

Noctor SC, Martìnez-Cerdeno V, Ivic L, Kriegstein AR. 2004. Cortical neurons arise in symmetric and asymmetric division zones and migrate through specific phases. Nat Neurosci. 7:136–144.

Nonaka-Kinoshita M, Reillo I, Artegiani B, Martínez-Martínez MÁ, Nelson M, Borrell V, Calegari F. 2013. Regulation of cerebral cortex size and folding by expansion of basal progenitors. EMBO J. 32(13):1817–1828.

Pacary E, Heng J, Azzarelli R, Riou P, Castro D, Lebel-Potter M, Parras C, Bell DM, Ridley AJ, Parsons M, et al. 2011. Proneural transcription factors regulate different steps of cortical neuron migration through Rnd-mediated inhibition of RhoA signaling. Neuron. 69:1069–1084.

Park DH, Hong SJ, Salinas RD, Liu SJ, Sun SW, Sgualdino J, Testa G, Matzuk MM, Iwamori N, Lim DA. 2014. Activation of neuronal gene expression by the JMJD3 demethylase is required for postnatal and adult brain neurogenesis. Cell Rep. 8(5): 1290–1299.

Pontious A, Kowalczyk T, Englund C, Hevner RF. 2008. Role of intermediate progenitor cells in cerebral cortex development. Dev Neurosci. 30:24–32.

Postiglione MP, Juschke C, Xie Y, Haas GA, Charalambous C, Knoblich JA. 2011. Mouse inscuteable induces apical-basal spindle orientation to facilitate intermediate progenitor generation in the developing neocortex. Neuron. 72:269–284.

Pounds S, Morris SW. 2003. Estimating the occurrence of false positives and false negatives in microarray studies by approximating and partitioning the empirical distribution of *p*-values. Bioinformatics. 19(10):1236–1242.

Ramos AD, Diaz A, Nellore A, Delgado RN, Park KY, Gonzales-Roybal G, Oldham MC, Song JS, Lim DA. 2013. Integration of genome-wide approaches identifies lncRNAs of adult neural stem cells and their progeny in vivo. Cell Stem Cell. 12(5):616–628.

Reillo I, Borrell V. 2012. Germinal zones in the developing cerebral cortex of ferret: ontogeny, cell cycle kinetics, and diversity of progenitors. Cereb Cortex. 9:2039–2054.

Reillo I, de Juan Romero C, García-Cabezas MÁ, Borrell V. 2011. A role for intermediate radial glia in the tangential expansion of the mammalian cerebral cortex. Cereb Cortex. 21(7):1674–1694.

Saito T. 2006. In vivo electroporation in the embryonic mouse central nervous system. Nat Protoc. 1:1552–1558.

Sanges R, Cordero F, Calogero RA. 2007. OneChannelGUI: a graphical interface to Bioconductor tools, designed for life scientists who are not familiar with R language. Bioinformatics. 23:3406–3408.

Satoh T, Takeuchi O, Vandenbon A, Yasuda K, Tanaka Y, Kumagai Y, Miyake T, Matsushita K, Okazaki T, Saitoh T, et al. 2010. The Jmjd3-Irf4 axis regulates M2 macrophage polarization and host responses against helminth infection. Nat Immunol. 11:936–944.

Schaeren-Wiemers N, Gerfin-Moser A. 1993. A single protocol to detect transcripts of various types and expression levels in neural tissue and cultured cells: in situ hybridization using digoxigenin-labelled cRNA probes. Histochemistry. 100:431–440.

Schmittgen TD, Livak KJ. 2008. Analyzing real-time PCR data by the comparative C(T) method. Nat Protoc. 3:1101–1108.

Sessa A, Mao CA, Colasante G, Nini A, Klein WH, Broccoli V. 2010. Tbr2-positive intermediate (basal) neuronal progenitors safeguard cerebral cortex expansion by controlling amplification of pallial glutammatergic neurons and attraction of subpallial GABAergic interneurons. Genes Dev. 24:1816–1826.

Sessa A, Mao CA, Hadjantonakis AK, Klein WH, Broccoli V. 2008. Tbr2 directs conversion of radial glia into basal precursors and guides neuronal amplification by indirect neurogenesis in the developing neocortex. Neuron. 60:56–69.

Shimojo H, Ohtsuka T, Kageyama R. 2008. Oscillations in notch signaling regulate maintenance of neural progenitors. Neuron. 58:52–64.

Shirazi Fard S, Kele J, Vilar M, Paratcha G, Ledda F. 2010. Tiam1 as a signaling mediator of nerve growth factor-dependent neurite outgrowth. PLoS One. 5(3):e9647.

Sholl D. 1953. Dendritic organization in the neurons of the visual and motor cortices of the cat. J Anat. 87(4):387–406.

Sinha S, Abraham S, Gronostajski RM, Campbell CE. 2000. Differential DNA binding and transcription modulation by three T-box proteins, T, TBX1 and TBX2. Gene. 258: 15–29.

Sola S, Xavier JM, Santos DM, Aranha MM, Morgado AL, Jepsen K, Rodrigues CM. 2011. p53 interaction with JMJD3 results in its nuclear distribution during mouse neural stem cell differentiation. PLoS One. 6:e18421.

Stühmer T, Anderson SA, Ekker M, Rubenstein JL. 2002. Ectopic expression of the Dlx genes induces glutamic acid decarboxylase and Dlx expression. Development. 129(1):245–52.

Thorvaldsdóttir H, Robinson JT, Mesirov JP. 2013. Integrative Genomics Viewer (IGV): high-performance genomics data visualization and exploration. Brief Bioinform. 14: 178–192.

Vasistha NA, García-Moreno F, Arora S, Cheung AF, Arnold SJ, Robertson EJ, Molnár Z. 2015. Cortical and clonal contribution of Tbr2 expressing progenitors in the developing mouse brain. Cereb Cortex. 25:3290–3302.

Wilkinson G, Dennis D, Schuurmans C. 2013. Proneural genes in neocortical development. Neuroscience. 253:256–273.

Wu Z, Irizarry RA. 2004. Preprocessing of oligonucleotide array data. Nat Biotechnol. 22:656–658.